Check for updates

Hydrological Processes

WILEY

RESEARCH ARTICLE OPEN ACCESS

Sensitivity of Stable Isotope Dynamics to Parametric and Conceptual Choices in Critical Zone Hydrological Modelling—A Case Study in Tropical Africa

Diego Chávez-Espinoza[1] | Sylvain Kuppel[2] | Christophe Peugeot[3] | Kei Yoshimura[4] | Christine Vallet-Coulomb[1]

[1]Aix-Marseille Univ., CNRS, IRD, INRAE, CEREGE, Aix-en-Provence, France | [2]Géosciences Environnement Toulouse, Univ. Toulouse, CNRS, IRD, UPS, CNES, Toulouse, France | [3]HSM, IRD, U. Montpellier, CNRS, IMT-Mines Alès, Montpellier, France | [4]Institute of Industrial Science, The University of Tokyo, Kashiwa, Japan

Correspondence: Christine Vallet-Coulomb (vallet@cerege.fr)

Received: 21 August 2025 | **Revised:** 5 November 2025 | **Accepted:** 11 November 2025

Keywords: EcH_2O-iso | evaporative kinetic fractionation | isotope-enabled ecohydrological modelling | sensitivity analysis | tropical hydrology | water stable isotopes

ABSTRACT

Tracer-enabled hydrological models are increasingly used to investigate water pathways by integrating hydrometric and stable isotope data. While quantifying the sensitivity of model outputs to global parameters is a common practice, structural sensitivity to empirical evaporative fractionation models is rarely explored, despite its critical influence on isotopic signatures, especially in evapotranspiration-dominated basins. In this study, we build upon the process-based distributed model EcH_2O-iso to quantify both types of isotopic sensitivities—conceptual, from changing the Craig and Gordon formulation used to quantify soil evaporative fractionation, widely applied in tracer-enabled hydrology, and parametric, from varying classical non-isotopic hydrodynamics parameters—in a tropical savanna basin in northern Benin with mixed land cover (fallow and forest). Looking at five locations and hydrological compartments, covering both local and basin scales, our results show that both types of sensitivities are of similar magnitude and significance, leading to changes in $\delta^{18}O$ outputs by several per mil. We further show that the choice of conceptual fractionation framework influences parametric sensitivities, especially locally, while at basin scales, sensitivities decrease as mixing may dominate over fractionation processes. Additionally, we highlight how vegetation-dependent root uptake further modulates the impact of modelling choices on tracer sensitivity. The differentiated relationships between inputs (parametric and conceptual) and outputs (isotopic time series) not only demonstrate the leverage of isotopic information to identify model configurations but also benchmark how evaporation fractionation formulations may alter the propagation of this information for estimating parameters controlling water storage and fluxes.

1 | Introduction

Tracer-enabled models are used to simulate the dynamics of stable isotopes (^2H and ^{18}O) in hydrological systems, from the local to the catchment scale, tracking water movement across the continuum of critical zone compartments and interfaces such as soil, vegetation, atmosphere, groundwater, and streams (Birkel and Soulsby 2015; IAEA 2023; Stadnyk and Holmes 2023; Tetzlaff et al. 2015). These models exhibit a wide range of architectures, each with varying assumptions about mixing within conceptual compartments. They range from simpler lumped and semi-lumped conceptual formulations (Hrachowitz, Savenije, Bogaard, et al. 2013; Knighton et al. 2017; Smith et al. 2016), to more complex semi and fully distributed process-based representations (Alaaho et al. 2017; Belachew et al. 2016; He et al. 2019; Kuppel

This is an open access article under the terms of the Creative Commons Attribution License, which permits use, distribution and reproduction in any medium, provided the original work is properly cited.

© 2025 The Author(s). *Hydrological Processes* published by John Wiley & Sons Ltd.

et al. 2018a; Stadnyk et al. 2013; Watson et al. 2024), some of which even detail soil water dynamics with a two-pore domain conceptualization (Sprenger et al. 2018, Snarski et al. 2025). Complementing these approaches, Storage Selection (SAS) function-based frameworks have been increasingly applied at the catchment scale to simulate tracer transport processes and estimate water residence times, providing a flexible alternative that captures mixing and storage dynamics without relying on detailed process representations (Benettin and Bertuzzo 2018; Evaristo et al. 2019; Harman and Xu Fei 2024; Knighton et al. 2019; Meira Neto et al. 2022; Rinaldo et al. 2015; Smith et al. 2018).

As water travels through the critical zone, its isotopic signature is influenced by physical phase transitions such as condensation, transpiration, evaporation, sublimation, freezing and thawing (Birkel and Soulsby 2015). Among these processes, evaporation tends to be the major source of isotopic fractionation (Jasechko 2019), which is commonly implemented in hydrological modelling approaches using the Craig-Gordon (C-G) model (Craig and Gordon 1965). Originally developed for open water bodies (Horita et al. 2008), the C-G model was also adapted to soil systems (e.g., Barnes and Allison 1983; Mathieu and Bariac 1996; Braud et al. 2005, 2009; Lin and Horita 2016) to quantify how the isotopic composition of water evolves during evaporation, accounting for equilibrium and kinetic isotope effects (Dubbert et al. 2013; Xiao et al. 2018).

While mixing processes tend to govern the evolution of water isotopic composition in humid, energy-limited environments, often resulting in fractionation effects being overlooked (Alaaho et al. 2017; Evaristo et al. 2019; Kirchner and Allen 2020), this is not the case in arid and highly seasonal regions, where direct evaporation plays a central role (Gat 1995; Gibson et al. 2016; Horita et al. 2008). In such contexts, accurately representing both equilibrium and kinetic components of isotopic fractionation becomes critical, as the C-G model may be particularly sensitive to how its environmental input variables are specified, thereby adding a layer of complexity to existing biophysical and hydrodynamic model parametrizations. A prime example is the isotopic composition of atmospheric vapour, a key driving variable challenging to measure accurately and thus rarely available as a direct input (Delattre et al. 2015; Dubbert et al. 2013; Horita et al. 2008), which is typically approximated by assuming isotopic equilibrium with local rainfall (Kumar and Nachiappan 1999). However, this simplification can introduce significant biases during the peak evaporation season, limiting its validity to certain temperate climates (Horita et al. 2008; Tremoy et al. 2012; Xiao et al. 2017). In this regard, despite the development of various experimental, analytical (Quade et al. 2018) and numerical modelling approaches (Braud et al. 2009), large uncertainties persist in estimating isotopic fractionation in soil water. This is mainly due to the ongoing debate and lack of consensus in the literature on the proper estimation of the kinetic fractionation factor (Braud et al. 2005; Dubbert et al. 2013), which potentially affects the accuracy of tracer-enabled models in simulating isotopic composition dynamics (Kuppel et al. 2018a).

Recognising this knowledge gap in hydrological modelling studies with stable isotopes, this study aims to improve the predictive power of tracer-enabled models through a careful examination of two sources of uncertainty: (1) the choice of model parameters, referred to here as parametric sensitivity, and (2) the conceptual assumptions used in calculating kinetic fractionation during soil evaporation, as represented by the C-G model variables, referred to here as conceptual sensitivity. We quantify the influence of both factors upon the simulation of isotopic signatures ($\delta^{18}O$ and $\delta^{2}H$) across different compartments of the critical zone, using a process-based ecohydrological model EcH_2O-iso in its current state of physical description of water and energy fluxes. This numeric tool is deployed in a highly seasonal tropical savanna basin, covering an area of approximately 10 000 km^2, where evapotranspiration is the main hydrological flux and is at the core of the system dynamics. Our driving hypotheses are (a) adopting a process-based and therefore flexible conceptualization of evaporative fractionation reduces the weight of parametric sensitivity and (b) parametric and conceptual sensitivities are modulated by the influence of land cover representation on hydrological dynamics. This study advances the predictive capability of tracer-enabled models by improving the identification of specific uncertainty sources (structural and parametric) and proposing strategies to reduce them.

2 | Data and Methods

2.1 | Model Description

2.1.1 | The EcH_2O-Iso Model

EcH_2O-iso is a process-based, distributed ecohydrological model developed to simulate energy and water fluxes along with vegetation dynamics in the critical zone, including transport and concentrations of conservative tracers ($\delta^{2}H$, $\delta^{18}O$ and Cl^{-}) and water ages (Douinot et al. 2019; Kuppel et al. 2018a; Maneta and Silverman 2013). The model domain, defined on a regular grid, and its drainage network are derived from a digital elevation model (DEM). Each grid cell, which can accommodate multiple land cover types, serves as the spatial unit where tightly coupled energy and water balance modules operate to drive simulations. The energy module uses a two-layer scheme (top of the canopy and surface) to partition energy fluxes into sensible, ground and latent heat, accounting for interception evaporation and transpiration via a Jarvis-type stomatal conductance model (Cox et al. 1998; Jarvis 1976). At the soil surface, the net available energy under each cover fraction is distributed into latent heat flux of evaporation (constrained by water availability and resistances), latent heat of snowmelt (if soil surface temperature exceeds 0°C), and sensible heat into the atmosphere, ground heat flux, sensible heat flux advected by throughfall and heat flux to the snowpack (Maneta and Silverman 2013). The water balance module simulates the movement and storage of water, employing a top-down, multi-layer approach, conceptualising water storage within compartments including the canopy, surface and subsurface, the latter divided into three hydraulic layers (Figure 1). It uses the Green-Ampt model approach for topsoil water infiltration and gravitational drainage to deeper layers, models lateral water transfer of overland flow along the local drainage direction, applying a kinematic wave approach for channel drainage and lateral groundwater flow across the subsurface layers. While

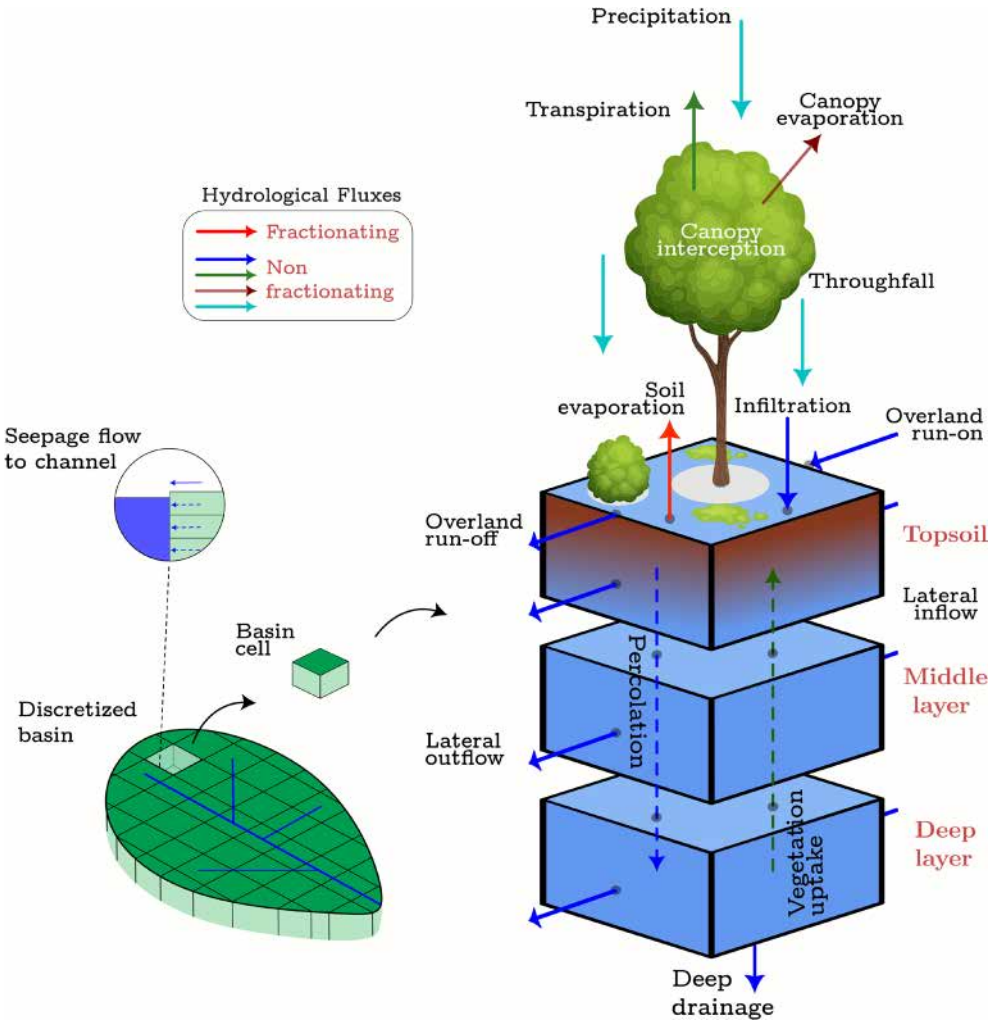

FIGURE 1 | Schematic representation of the hydrological fluxes simulated by EcH2O-iso at the grid cell level, where diverse vegetation types can coexist within a single cell alongside bare soil. Hydrological connectivity is maintained through lateral flow, linking surface and subsurface water movement between neighbouring cells. The model represents the soil column as three distinct layers: topsoil, middle and deep. Seepage flows from adjacent soil layers into river channel cells. Isotopic fractionation from soil evaporation is modelled using the Craig-Gordon approach limited to the topsoil layer. Water intercepted by the canopy of any vegetation type is assumed to fully evaporate, preventing infiltration into the soil. Meanwhile, throughfall, the fraction of precipitation that reaches the ground after passing through the canopy, retains the isotopic composition of precipitation from the same time step. Groundwater compartment integrates the storage-weighted isotopic composition of all soil compartments above field capacity.

the energy module calculates the rate of transpiration, the water module tracks its source within the root uptake profiles. Soil water used for transpiration draws from different soil layers according to a recently implemented root water uptake profile calculation based on Ohm's law of potential-driven flow: the ratio between (conductive) soil water potential and (resistive) depth from the surface dynamically shapes the relative contribution of each subsurface layer, which can differ among individuals of the same species according to their topographic positions (Fan et al. 2017; Miguez-Macho and Fan 2021).

2.1.2 | Stable Isotope Tracking

Isotope tracking in EcH$_2$O-iso is implemented through a mass balance approach, using lateral and vertical fluxes computed between hydrological compartments and grid cells at each time step. The model locally assumes complete mixing within each hydrological compartment and timestep at the grid cell levels. Following the formulation in Smith et al. (2020), Equations (1) and (2) describe the mixing of tracer signatures and volumes within storage layers. In Equation (1), δ_{old} and δ_{new} denote the tracer signature (δ^2H or δ^{18}O) before and after mixing, respectively; F_{in} and δ_{in} correspond to the incoming water flux and its associated signature, and Δt is the simulation time step. V_{mix} represents an intermediate mixing volume taking into account sub-timestep for change in mixing volume in each storage layer. This volume is further defined in Equation (2), where V_{old} is the initial stored volume and F_{out} is the outgoing water flux.

$$\delta_{new} = \frac{\delta_{old}\left(V_{mix} - 0.5.F_{in}\Delta t\right) + \delta_{in}F_{in}\Delta t}{V_{mix} + 0.5.F_{in}\Delta t} \quad (1)$$

$$V_{mix} = 0.5.\left(V_{old} + F_{in}\Delta t + max\left(V_{old} - F_{out}\Delta t, 0\right)\right) \quad (2)$$

In the topsoil layer (Figure 1), evaporative fractionation is simulated as follows:

$$\delta_{SoilL1}^{t+\Delta t} = \delta^* - \left(\delta^* - \delta_{Soil\ L1}^{t}\right).f^m \tag{3}$$

which is derived from the Craig-Gordon (C-G) model and represents the isotopic changes in soil water due to evaporation between two successive time steps. The interaction of three factors is represented in Equation (3): the residual water fraction after evaporation f (Equation 4); the limiting isotopic composition δ^* defined by local atmospheric conditions in ‰ (Equation 5) (Gat and Levy 1978); and the dimensionless exponent m governing kinetic isotopic enrichment (Equation 6) (Allison and Leaney 1982; Welhan and Fritz 1977).

$$f = V_{SoilL1}^{t+\Delta t} / V_{SoilL1}^{t} \tag{4}$$

$$\delta^* = \frac{h_a\delta_a + h_s\varepsilon^+ + \varepsilon_k}{h_a - \left(h_s\varepsilon^+ + \varepsilon_k\right).10^{-3}} \tag{5}$$

$$m = \frac{h_a - \left(h_s\varepsilon^+ + \varepsilon_k\right).10^{-3}}{h_s - h_a + \varepsilon_k.10^{-3}} \tag{6}$$

where $V_{SoilL1}^{t+\Delta t}$ and V_{SoilL1}^{t} are, respectively, the topsoil water storage after and before direct evaporation. Both δ^* and m follow Good et al. (2014) formulations to explicitly incorporate vapour and soil water status into the C-G model, first through using the relative humidity of the ambient atmosphere (h_a) and of the air within soil pores (h_s). In Equation (7), h_a is normalised to the saturated vapour pressure e^* at the soil surface temperature, where T_a is the air temperature and T_s is the soil surface temperature derived from the energy balance equation solved by EcH$_2$O-iso. Following Maneta and Silverman (2013), Equation (8) estimates the relative humidity of the air within soil pores h_s, incorporating the soil moisture function β, which is defined by Lee and Pielke (1991) as a function of volumetric soil moisture θ and field capacity θ_{fc}, and is presented in Equation (9).

$$h_a = h_{a,measured}.\frac{e^*\left(T_a\right)}{e^*\left(T_s\right)} \tag{7}$$

$$h_s = \beta + (1-\beta).h_a \tag{8}$$

$$\beta = min\left(1, \frac{1}{4}\left[1 - cos\left(\pi\frac{\theta}{\theta_{fc}}\right)\right]^2\right) \tag{9}$$

Further, the equilibrium separation ε^+ is derived from the air-temperature-dependent equilibrium fractionation factor α^+ between liquid and vapour phases (Equation 10), using the empirical polynomial functions in Horita and Wesolowski (1994). The kinetic separation ε_k arises from water vapour transport through the three C-G model layers, namely interface, laminar and turbulent (Horita et al. 2008). This transport is proportional to a dimensionless factor n (Equation 11), which characterises the aerodynamic regime above the liquid–vapour interface, and the diffusivity ratio $^{D_i}/_{D}$, where D_i is the diffusion coefficient of the isotopic species of interest (i.e., $^1H^2H^{16}O$ and $^1H^1H^{18}O$) and D that of the reference isotopic species (i.e., $^1H_2{}^{16}O$). Merlivat (1978) experimentally determined $^{D_i}/_{D}$ as 0.9757 for $D_{\,^1H^2H^{16}O} / D_{\,^1H_2^{16}O}$ and 0.9727 for $D_{\,^1H^1H^{18}O} / D_{\,^1H_2^{16}O}$, values widely adopted in isotope studies (i.e., Barnes and Allison 1983; Good et al. 2014; Pfahl and Wernli 2009; Quade et al. 2018; Soderberg et al. 2012). Meanwhile, n is derived from Equation (12) using soil water content θ, soil porosity ϕ and residual water content θ_r in the topsoil, which correspond to the first hydraulic layer of EcH$_2$O-iso.

$$\varepsilon^+ = \left(\alpha^+ - 1\right).10^3 \tag{10}$$

$$\varepsilon_k = \left(h_s - h_a\right).n.\left(1 - \frac{D_i}{D}\right) \tag{11}$$

$$n = 1 - 0.5.\frac{\left(\theta - \theta_r\right)}{\left(\phi - \theta_r\right)} \tag{12}$$

If input data are unavailable, the air isotope composition δ_a can be derived from precipitation isotopic signature δ_{rain} assuming isotopic equilibrium, which is the default approach in EcH$_2$O-iso (Gat 1995; Gibson and Reid 2014):

$$\delta_a = \frac{\delta_{rain} - \varepsilon^+}{\alpha^+} \tag{13}$$

2.1.3 | Conceptualizations of Craig-Gordon Variables

Based on the basic formulation of the C-G approach to model the evaporative fractionation, several implementations have been adopted among the many existing types of tracer-enabled critical zone models over the last two decades. Our literature review notably pointed at a subset of key driving variables of the C-G model—*hs*, *n* and δ_a, already defined in Section 2.1.2—to which fractionation may be quite sensitive, yet with contrasting quantification depending on the models; from fixed and idealised values or relationships to more refined formulations (Table S1). Here we attempt to explore this diversity by using two alternative conceptualizations of each of these three C-G variables in an extended version of the C-G module in the EcH$_2$O-iso model, as summarised in Table 1.

TABLE 1 | Representations of C-G input variables in the EcH2O-iso evaporative fractionation module.

Craig-Gordon input variables	Conceptualization	Notation
hs	Permanently saturated vapour	*h*1
	Lee and Pielke (1991)	*hv*
n	Fully diffusive transport	*n*1
	Mathieu and Bariac (1996)	*nv*
δ_a	Isotopic equilibrium	δ_{a-eq}
	Input forcing	$\delta_{a-input}$

Note: Their combinations result in 8 possible conceptual frameworks.

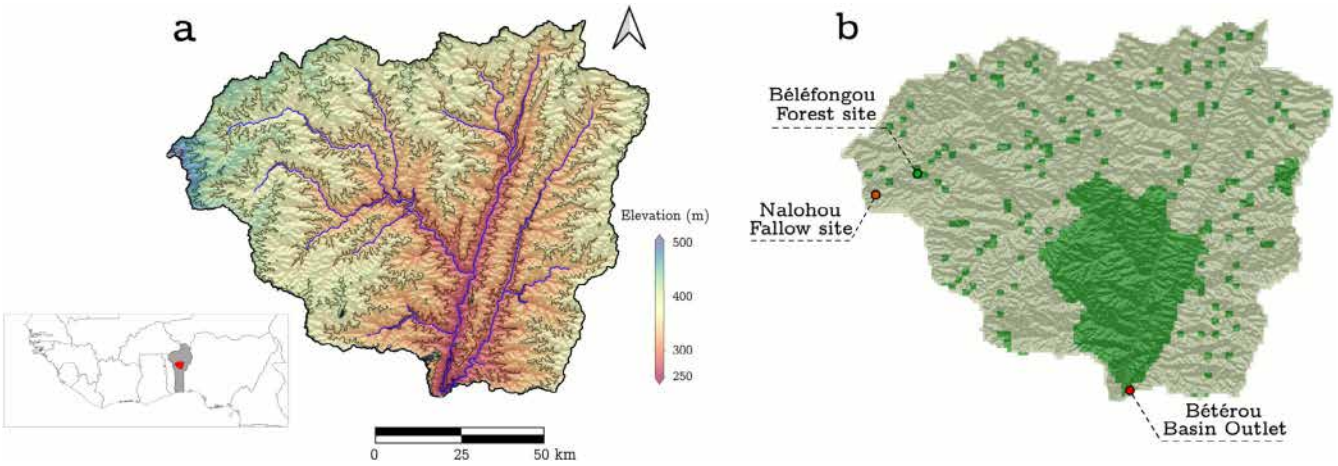

FIGURE 2 | (a) Topographic map of the Bétérou basin, displaying the main river network and basin relief. (b) Simplified land cover map, reclassified into forest and fallow categories, derived from 2-km resolution West Africa Land Use Land Cover map (Tappan et al. 2016), showing the locations of the AMMA-CATCH experimental sites at Béléfongou and Nalohou experimental sites.

For *hs*, the first conceptualization, denoted *h*1, assumes that $hs = 1$, which corresponds to the general C-G formulation, that is, ε^+ is not weighted in Equations (5) and (6). In the Lee and Pielke (1991) formulation, it corresponds to the topsoil remaining at field capacity or above ($\theta \geq \theta_{fc}$ in Equation (8)) throughout simulations. The second conceptualization, referred to as *hv*, accounts for dynamic variations of *hs* as a function of topsoil moisture changes (Equation 8).

Similarly, for *n*, the first conceptualization, *n*1, assumes a purely diffusional transport ($n = 1$), corresponding to a permanently dry topsoil ($\theta = \theta_r$ in Equation 12), whereas the second, identified as *nv*, reflects variations in simulated soil moisture, following Equation (12).

Regarding δ_a, while crucial for deriving the limiting isotopic composition δ^* from local atmospheric conditions (Equation 5) and the progressive kinetic fractionation during evaporation (Equation 6), its estimation is challenging due to technical complexities in both sampling and analysis (Soderberg et al. 2012). Without available data, it is often assumed that equilibrium exists between vapour and precipitation to estimate δ_a (Equation 13). However, several studies have argued that this common premise does not always hold, particularly in arid or semi-arid regions with high evaporation rates, and where δ_a may deviate from the equilibrium assumption during long dry periods (Gibson et al. 2016; Horita et al. 2008; Mercer et al. 2020; Penchenat et al. 2020; Stewart 1975). In our study, we consider the first conceptualization (δ_{a-eq}) based on the precipitation—vapour isotopic equilibrium assumption, which is the standard formulation in the EcH_2O-iso model. Alternatively, the second conceptualization ($\delta_{a-input}$) involves the use of δ_a as an input forcing, derived from simulations of the Isotopic Global Spectral Model (IsoGSM), an isotope-enabled Atmospheric General Circulation Model (AGCM) developed by Yoshimura et al. (2008). We leverage recent advances, notably the high-resolution IsoGSM-T248 configuration introduced by Bong et al. (2024), which have improved its capacity to represent isotopic variability at finer spatial scales, through a water isotope budget approach.

2.2 | Study Site and Datasets

2.2.1 | Study Site

The Bétérou basin is in central Benin within the upper Ouémé basin (Figure 2). Monitored by the AMMA-CATCH critical-zone observatory (Galle et al. 2018), this region covers approximately 10 000 km^2 and is geographically bounded by longitudes 1°30′ E to 2°49′ E and latitudes 9°10′ N to 10°12′ N. Repeated pedimentation cycles have transformed the area into a peneplain with an average slope of 2.5%, marked by occasional irruption of steep inselbergs throughout the landscape (Bormann and Diekkrüger 2003; Cornelissen et al. 2013). Elevations within the basin range from 250 to 617 m (Figure 2a). This region is characterised by a tropical wet savanna, receiving an average precipitation of 1200 mm year^{-1}, falling during the unimodal wet season from April to October, an average annual temperature of 25°C and a potential evapotranspiration rate of 1500 mm year^{-1}. The Ouémé River has an intermittent flow regime, with discharges occurring from late June to January, coinciding with and following the rainy season (Le Lay et al. 2007).

The study area lies within the Benino-Nigerian Shield, comprising a Precambrian crystalline basement which dominates the geological landscape of northern Benin (El-Fahem 2008; Kotchoni et al. 2019), and is characterised by the presence of tropical ferruginous soils (Galle et al. 2018). Vegetation in the Bétérou basin consists of a mosaic of clear forests, savannahs and croplands (Galle et al. 2018).

2.2.2 | Datasets

Climatic forcings such as air temperature, relative humidity, wind speed and incoming longwave and shortwave radiation (Figure 3c–g) were obtained from the ERA5-Land Hourly reanalysis dataset (Muñoz Sabater 2019), from the European Centre for Medium-Range Weather Forecasts (ECMWF), covering the basin at a spatial resolution of 0.1°×0.1° (~9×9 km^2). Precipitation records were obtained from the AMMA-CATCH hydrological

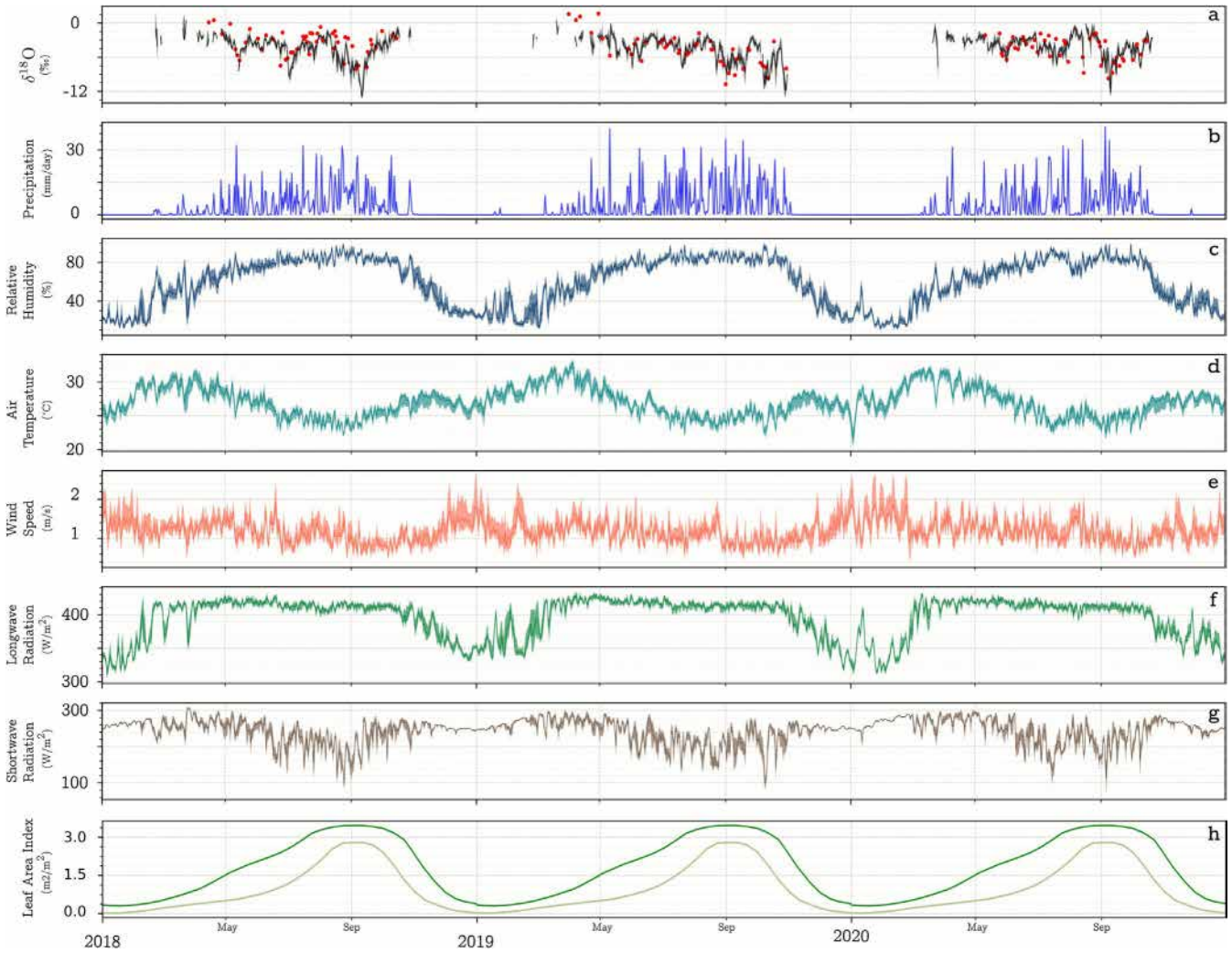

FIGURE 3 | Daily isotopic and climatic forcings used as inputs for the model for the 2018–2020 period. The time series envelopes capture the range of values from the ERA5-Land reanalysis and IsoGSM datasets across the basin, with solid lines indicating the median value at each time step. Panel (a) presents precipitation isotopic composition from IsoGSM alongside observations at the Nalohou experimental site (red dots), while (b) illustrates mean precipitation over the basin. Panels (c) to (g) display climatic variables derived from the ERA5-Land dataset, while panel (h) shows the LAI for forest and fallow, depicted in dark and light green, respectively.

monitoring network, with precipitation records at 5-min intervals. The isotopic signatures of precipitation and atmospheric water vapour were derived from the isotope-enabled IsoGSM-T248 model, which provides continuous, high-resolution datasets (about 0.47°, or 52.5 km at the Equator) at a daily time step. Figure 3a illustrates the good agreement between the isotopic composition of precipitation and the samples collected at the Nalohou station, as shown also in Figure S1. The land cover map of the basin was derived from the West Africa Land Use Land Cover map (Tappan et al. 2016), with vegetation categories simplified into fallow and forest. The Leaf Area Index (LAI) time series for both categories were obtained (Figure 3h) from Lohou et al. (2014), based on remote sensing and hemispherical photography at the Nalohou and Béléfongou experimental sites (Figure 2b). Due to the lack of site-specific observations and significant gaps in satellite-derived LAI data during the rainy season caused by persistent cloud cover, the 2005–2008 data were averaged to produce a single representative daily series per land cover type. This approach is further justified by the low inter-annual variability in the LAI of the dominant tree cover, supporting its use as model input.

2.2.3 | Simulation Set-Up

The Bétérou basin landscape was represented using a 1-km resolution DEM derived from the Shuttle Radar Topography Mission (NASA JPL 2013). EcH$_2$O-iso simulations ran daily over a 5-year period, from January 2016 to December 2020. To stabilise the initial hydrological conditions of the model, a 2-year warm-up phase, from January 2016 to December 2017, was considered and later excluded from the analysis. Additionally, a uniform initial isotopic composition was assigned to all soil compartments to help isotopic series stabilization during the warm-up phase ($\delta^2H = -20.5‰$, $\delta^{18}O = -3.5‰$). Climatic forcings (see Section 2.2.2) were aggregated into daily mean values, with precipitation data spatially distributed using Thiessen polygons, while isotopic forcings were applied uniformly across the model domain. The hydrodynamic, energy-related and vegetation parameters of primary importance for the simulated Bétérou basin were specified as listed in Table 2, with bounds allowing open exploration of the parameter space. All other EcH$_2$O-iso parameters, considered as secondary or redundant, were kept at their

TABLE 2 | EcH_2O-iso model parameters and their ranges.

Parameter	Description	Units	Min	Max
Soil parameters				
D_{L1}	Thickness of the 1st hydrological layer	m	0.05	0.3
D_{L2}	Thickness of the 2nd hydrological layer	m	0.1	1
D_{soil}	Total soil depth	m	10	30
θ_{L1}	Porosity of the 1st hydrological layer	$m^3 m^{-3}$	0.2	0.5
θ_{L2}	Porosity of the 2nd hydrological layer	$m^3 m^{-3}$	0.2	0.5
θ_{L3}	Porosity of the 3rd hydrological layer	$m^3 m^{-3}$	1E-02	3E-01
K_{L1}	Saturated horizontal hydraulic conductivity of the 1st hydrol. layer	$m^1 s^{-1}$	1E-06	1E-02
K_{L2}	Saturated horizontal hydraulic conductivity of the 2nd hydrol. layer	$m^1 s^{-1}$	1E-06	1E-02
K_{L3}	Saturated horizontal hydraulic conductivity of the 3rd hydrol. layer	$m^1 s^{-1}$	1E-08	1E-03
$Khratio_{L1}$	Anisotropy of the 1st hydrological layer	—	0.1	10
$Khratio_{L2}$	Anisotropy of the 2nd hydrological layer	—	0.1	10
$Khratio_{L3}$	Anisotropy of the 3rd hydrological layer	—	0.1	10
$\lambda_{BC\text{-}L1}$	Brook-Corey lambda of the 1st hydrological layer	—	2	12
$\lambda_{BC\text{-}L2}$	Brook-Corey lambda of the 2nd hydrological layer	—	2	12
$\lambda_{BC\text{-}L3}$	Brook-Corey lambda of the 3rd hydrological layer	—	2	12
ψae_{L1}	Air-entry pressure head of the 1st hydrological layer	m	0.1	0.8
ψae_{L2}	Air-entry pressure head of the 2nd hydrological layer	m	0.1	0.8
ψae_{L3}	Air-entry pressure head of the 3rd hydrological layer	m	0.1	0.8
θr_{L1}	Residual soil moisture of the 1st hydrological layer	$m^3 m^{-3}$	0.03	0.15
θr_{L2}	Residual soil moisture of the 2nd hydrological layer	$m^3 m^{-3}$	0.03	0.15
θr_{L3}	Residual soil moisture of the 3rd hydrological layer	$m^3 m^{-3}$	0.03	0.15
$gwseep_{L1}$	Groundwater seepage from the 1st hydrological layer	—	1E-04	1E-01
$gwseep_{L2}$	Groundwater seepage from the 2nd hydrological layer	—	1E-04	1E-01
$gwseep_{L3}$	Groundwater seepage from the 3rd hydrological layer	—	1E-04	1E-01
n	Manning's roughness coefficient	—	10	100
α_s	Soil albedo	—	0.1	0.3
Vegetation parameters				
gs_{max}	Maximal stomatal conductance	$m^1 s^{-1}$	0.001	0.015
gs_{light}	Stomatal sensitivity to light	—	0	300
gs_{vpd}	Stomatal sensitivity to vapour pressure deficit	Pa^{-1}	1E-05	2E-03
T_{opt}	Optimal photosynthesis temperature	°C	15	30

(Continues)

TABLE 2 | (Continued)

Parameter	Description	Units	Min	Max
T_{max}	Maximum temperature of comfort for the species	°C	35	40
T_{min}	Minimum temperature of comfort for the species	°C	1	10
LWP_{low}	Soil moisture suction threshold for zero stomatal conductance	m	200	600
LWP_{high}	Soil moisture suction threshold for stomatal conductance	m	40	150
CWS_{max}	Maximum interception storage per unit LAI	m	1E-05	4E-04
K_{Beer}	Beer's light extinction coefficient	—	0.3	0.8
α_c	Effective canopy albedo	—	0.1	0.3

Note: Soil parameters for each model layer (Topsoil L1, Middle L2 and Deep L3) correspond to uniform values across the basin. The value of each vegetation parameter may differ between the fallow and forest cover. The parameter range encompasses the possible values for both cover types.

default values. Each subsurface layer was assumed to share identical parameterization across the entire basin, with their thicknesses provided in Table 2. This spatial uniformity also applied to the two land cover types, fallow and forest, as shown in the simplified land cover map in Figure 2b, in terms of vegetation parameters and vegetation dynamics forcings (i.e., LAI time series shown in Figure 3h). A no-flow condition was imposed at the bottom of the deeper soil layer, assuming that drainage in the deeper critical zone is negligible given the geological context and the spatial scales here considered (Séguis et al. 2011; Vouillamoz et al. 2015). Analysis focused solely on $\delta^{18}O$ model outputs since $\delta^{2}H$ is expected to show similar temporal dynamics. Moreover, the wet season was defined as the period from April 1 to October 15, to segment the analysis period.

2.3 | Sensitivity Analysis

In modelling, the process of assessing how variations in model formulations, inputs and parameters values influence model outputs is known as sensitivity analysis (Saltelli et al. 2007). It rigorously quantifies the contribution of each influencing factor to system behaviour, aiding in the identification of the most sensitive parameters and inputs that significantly impact model predictions (Abbas et al. 2024; Bittner et al. 2021). The inspected sensitivity may change depending on the specific aspect of the model output being considered (Holmes et al. 2023). Sensitivity analysis also evaluates model result reliability and can identify periods of heightened model sensitivity (McGuire and McDonnell 2006). Focusing on main factors determining simulation results allows concentrating resources on improving their observation accuracy (Li et al. 2023). Here, our analysis distinguishes between the quantification of parametric sensitivity and conceptual sensitivity, as summarised in Figure 4 and explained in detail below. We do not consider other potential source of uncertainties such as model inputs (e.g., climatic forcings) and the impact of spatial averaging notably explored in Smith et al. (2021). In all cases explored, we primarily analysed 5 types of simulated $\delta^{18}O$ time series: topsoil and groundwater at two sites (forest and fallow cells), and stream discharge at the basin outlet. Site locations are shown in Figure 2b. This method was also applied to d-excess ($\delta^{2}H - 8.\delta^{18}O$), as commented in Sections 3 and 4.

2.3.1 | Parametric Sensitivity

Parametric sensitivity is probably the most used quantitative sensitivity analysis. Here we use the Morris method (Morris 1991; Sohier et al. 2014), a common, parsimonious approach for sensitivity analysis of model parameters, satisfactorily used in previous studies involving EcH_2O-iso (Gillefalk et al. 2021; Kuppel et al. 2018b; Neill et al. 2021; Smith et al. 2019; Yang et al. 2023). It identifies the most influential parameters by calculating elementary effects (EEs) and ranking model output changes when varying one parameter at a time. Parameter variation occurs within prescribed intervals, starting with the generation of random "centre points" in the parameter space using Latin hypercube sampling (McKay et al. 1979) to improve representativity. From each centre point, a "random trajectory" approach perturbs parameters one at a time in sequence, adding or subtracting half the size of its allowed interval, depending on whether its initial value falls in the lower or upper half of the interval, respectively (Sohier et al. 2014). After each perturbation, the new set becomes the starting point for the next change. For n parameters, this results in $n+1$ parameter sets (the initial set and the n perturbed sets) and simulations per centre point. The raw effect of each parameter is quantified by comparing model outputs before and after perturbation, using a chosen metric (see below). The EE of a parameter is then computed as the average of its raw effects across all trajectories.

We generated 8 Morris centre points, following Sohier et al. (2014), applied to 48 model parameters (26 for (sub)surface, and 2*11 for 2 cover types). This corresponds to $k=8$ and $p=48$ in Figure 4, with parameter bounds listed in Table 2. This process resulted in $k^{*}(p+1)=392$ parameter sets for analysis. The magnitude of sensitivity results is expressed in ‰ and is based on statistical analysis of the isotopic composition of five compartments: groundwater and topsoil for two representative grid cells (forest and fallow), and streamflow at the basin outlet.

For individual parameter sensitivity, changes in outputs are measured using pairwise RMSE (i.e., between two simulated outputs differing only by one parameter value in a given trajectory), with the EE (μ^{*}) of each parameter calculated as the mean

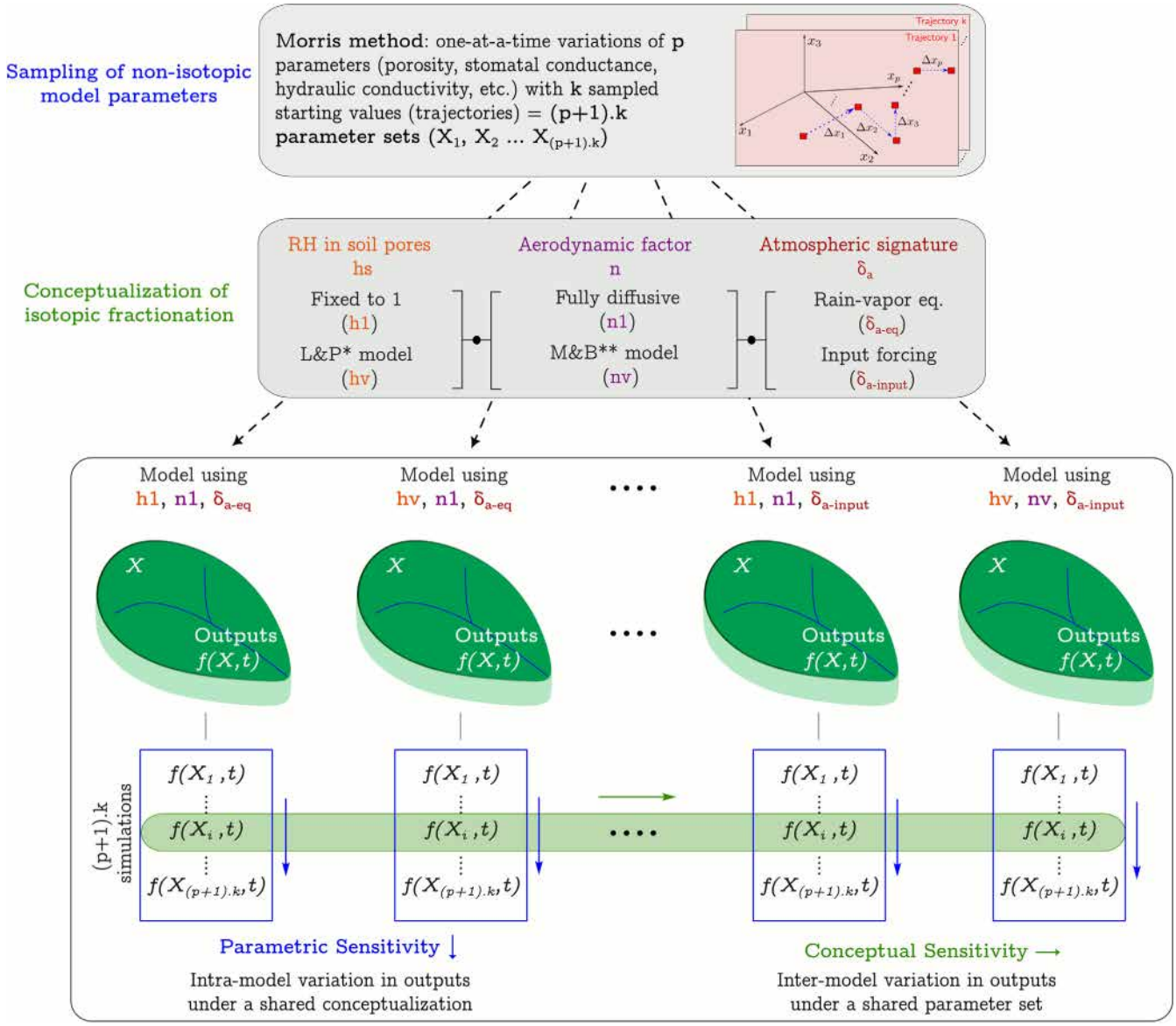

FIGURE 4 | Illustration of the strategy used to explore parametric and conceptual sensitivity. Parametric sensitivity is assessed by varying non-isotopic model parameters using the Morris method, while keeping the C-G conceptual framework fixed (i.e., a specific combination of *hs*, *n* and δ_a among the 8 possible). Conversely, conceptual sensitivity is assessed by comparing the 8 C-G conceptual frameworks (i.e., different assumptions for *hs*, *n* and δ_a) using the same parameter set (illustrated by the horizontal green band). In both cases, comparisons are based on the simulated isotopic composition (see text for details). *L&P and **M&B refer to the models of Lee and Pielke (1991) and Mathieu and Bariac (1996), respectively (see Table 1).

of these RMSE values across all trajectories for a given output and conceptual framework (Figure 4).

Additionally, for each of the 8 possible combinations of C-G input variables, we quantified the overall intra-model dispersion (ID) in ‰, calculated across all 392 sampled parameter sets, for each simulated $\delta^{18}O$ output:

$$ID = \frac{1}{N_{eval}} \sum_{i=1}^{N_{eval}} \left[M_{95}(t_i) - M_5(t_i) \right] \ldots \quad (14)$$

where $M95(t_i)$ and $M5(t_i)$ are the 95th and 5th percentiles of the ensemble of $\delta^{18}O$ simulations at time step i during a given evaluation period, and N_{eval} is the length of this period. This analysis was conducted over the entire period (1096 days, i.e., 2018–2020) as well as separately for the dry (502 days) and wet seasons (594 days).

2.3.2 | Conceptual Sensitivity

The conceptual sensitivity of the five $\delta^{18}O$ outputs considered here was quantified for each of the $\binom{8}{2} = 28$ possible pairs of conceptual frameworks (see Table 1 and Figure 4), using a two-step approach. First, for each of the 392 parameter sets generated (see Section 2.3.1), we computed the RMSE between outputs from models differing only in their C-G conceptual framework; for instance, this included comparing streamflow

$\delta^{18}O$ time series simulated under the $h1$-$n1$-δ_{a-eq} and $h1$-nv-δ_{a-eq} frameworks. Second, the overall conceptual sensitivity was calculated by averaging these RMSE values across parameter sets.

3 | Results

3.1 | Parametric Sensitivity

Figure 5 shows the EEs (μ^*) on water $\delta^{18}O$, focusing only on parameters with μ^* greater than or equal to 0.5‰ for at least one conceptual framework and compartment. This threshold corresponds to the upper bound of analytical precision commonly reported for pore water stable isotope measurements (Sprenger et al. 2016). As the most influential sets of parameters for each compartment remain essentially unchanged across seasons (see Figures S2 and S4 for d-excess), only results from the full period are presented for analysis.

The topsoil isotopic signature is more sensitive to soil physical parameters (names shown in black in Figure 5) under fallow than forest cover, irrespective of the conceptual framework. This sensitivity mainly affects parameters controlling water dynamics and storage in the fallow-covered compartment, including the Brook-Corey pore size index (λ_{BC-L1}), porosity (θ_{L1}), air-entry pressure head (ψae_{L1}), and residual soil moisture (θr_{L1}), which remain sensitive under forest cover but with reduced influence. Additionally, under fallow cover, sensitivities above 0.5‰ appear in deeper subsurface parameters (model layer L3), particularly porosity (θ_{L3}) and saturated hydraulic conductivity (K_{L3}), and to a lesser degree in the middle layer (L2) with parameters such as porosity (θ_{L2}), saturated hydraulic conductivity (K_{L2}) and depth (D_{L2}), which show little or no sensitivity under forest cover. This pattern also appears in groundwater, but less pronounced, with parameters θ_{L3} and K_{L3} standing out. Regarding vegetation parameters (green labels, Figure 5), effects on topsoil are similar across covers, yet this group includes those to which the forest-covered cell is most sensitive (compared to subsurface

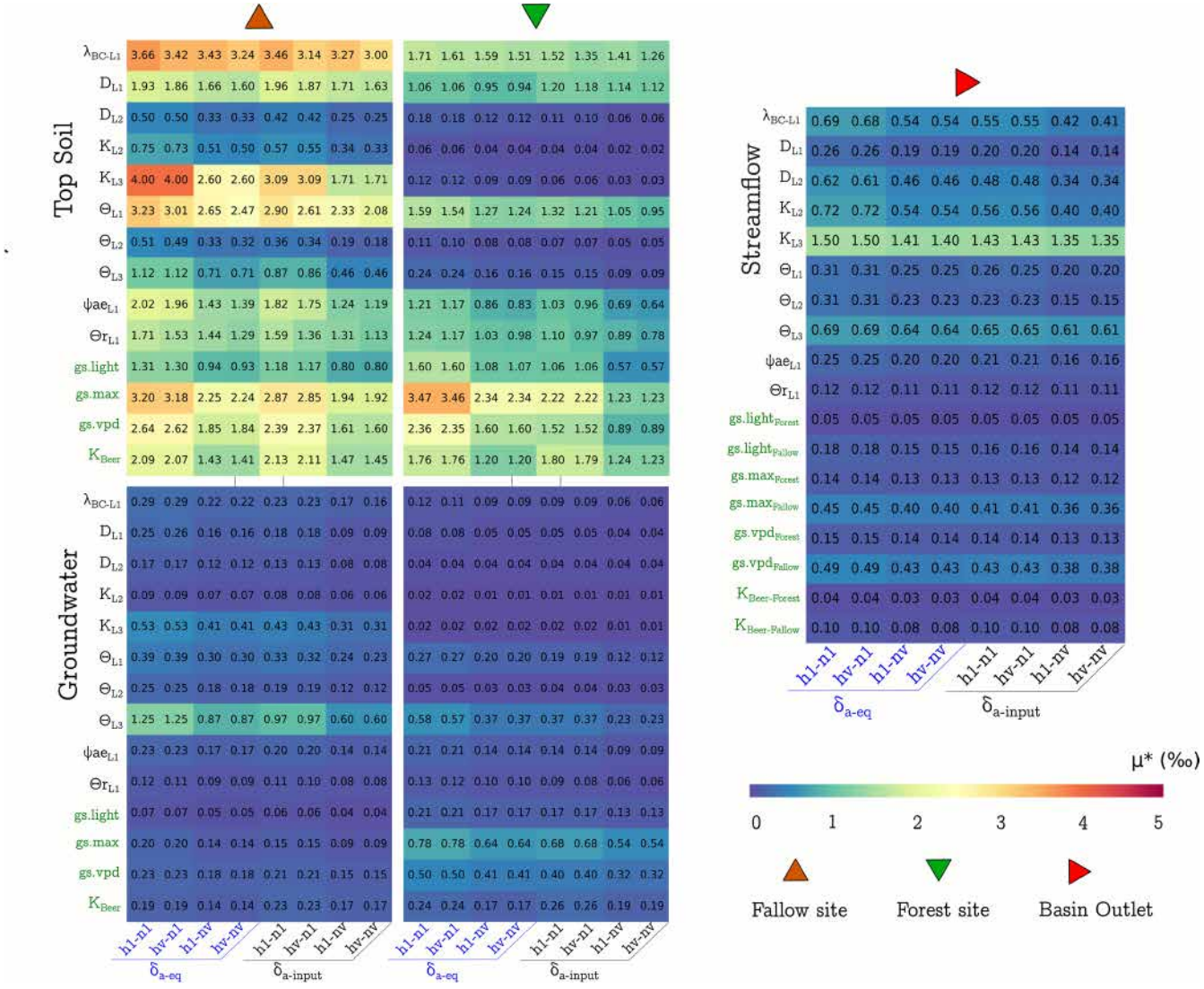

FIGURE 5 | Elementary effects (μ^*) of model parameters on water isotopic composition ($\delta^{18}O$) over the full simulation period, evaluated under various soil evaporative fractionation conceptualizations for topsoil and groundwater at fallow (orange marker, left column) and forest (green marker, centre column) sites, and for streamflow at the basin outlet (red marker, right column). The subscripts L1, L2 and L3 denote the topsoil, middle, and deep soil layers (see Figure 1). Parameter names shown in black denote soil parameters; those in green indicate vegetation parameters.

parameters for this cover), particularly the maximum stomatal conductance (gs_{max}). Moreover, the parameter controlling light attenuation (K_{Beer}), linked to LAI, shows slightly greater sensitivity under fallow cover than under forest. Regarding groundwater $\delta^{18}O$ signatures, forest vegetation parameters controlling stomatal conductance (gs_{light}, gs_{max} and gs_{vpd}) have a more attenuated effect than in topsoil; however, this groundwater sensitivity remains higher than at the fallow site. At the basin outlet, the streamflow isotopic signal is primarily influenced by subsurface parameters, particularly the saturated hydraulic conductivity of the deepest subsurface layer (K_{L3}) and, to a lesser extent, by that of the intermediate layer (K_{L2}) and by storage capacity (especially θ_{L3} and D_{L2}) and topsoil pore distribution (λ_{BC-L1}) along the subsurface profile. Vegetation parameters exert a smaller influence, with only those fallow-related ones nearing the 0.5‰ threshold previously mentioned.

Figure 5 also shows that parametric sensitivity decreases for most parameters as the C-G conceptual framework variables h and n follow a dynamic formulation (hv and nv), and δ_a departs from the default assumption of equilibrium (δ_{a-eq}). This reduction is most evident in the topsoil compartment, less so in groundwater and streamflow, where the sensitivity to some parameters remains stable or changes only slightly regardless of the C-G conceptual framework used. Similar patterns for d-excess, albeit with higher values ranges in inter-parameters sensitivity ranking and inter-framework relative changes (Figure S4).

Figure 6 provides a more comprehensive overview by presenting the dispersion of simulated $\delta^{18}O$ across all sampled parameter sets, organised by compartment and conceptual framework as in Figure 5. The dispersion of $\delta^{18}O$ in topsoil and groundwater is generally greater under fallow than forest cover, regardless of the C-G conceptual framework used. This pattern is more evident in the topsoil compartment, where isotopic fractionation directly takes place, especially during the dry season, with dispersion reaching up to 18‰ under fallow (up to 90‰ in d-excess, Figure S5). In contrast, $\delta^{18}O$ dispersion in groundwater and streamflow at the outlet is markedly lower, not exceeding 5‰.

We quantified the effect of the conceptual frameworks on the parametric sensitivity by testing different formulations for the fractionation variables (hs, n and δ_a) individually, focusing on parametric sensitivity changes. This approach shows that the largest effects occur in topsoil under fallow cover. Over the full simulation period, the dynamic formulation of hs ($h1$ vs. hv), when combined with $n1$ and $\delta_{a-input}$, reduces parameter sensitivity by up to 0.32‰, led by λ_{BC-L1} (Figure 5), and decreases overall dispersion by up to 0.33‰ (Figure 6). Varying δ_a (δ_{a-eq} vs. $\delta_{a-input}$), when combined with hv and $n1$, has a stronger effect, lowering individual parametric sensitivity by up to 0.91‰, led by K_{L3} (Figure 5), and decreasing overall dispersion by up to 2.79‰ (Figure 6). Finally, refining the representation of n ($n1$ vs. nv), when combined with $h1$ and δ_{a-eq}, produces the largest reductions in parameter sensitivity, reaching up to 1.40‰, led by K_{L3} (Figure 5) and an overall dispersion reduction of up to 4.01‰ (Figure 6). Results for d-excess, obtained for those conceptual frameworks and parameters, show higher reductions in parametric sensitivity and

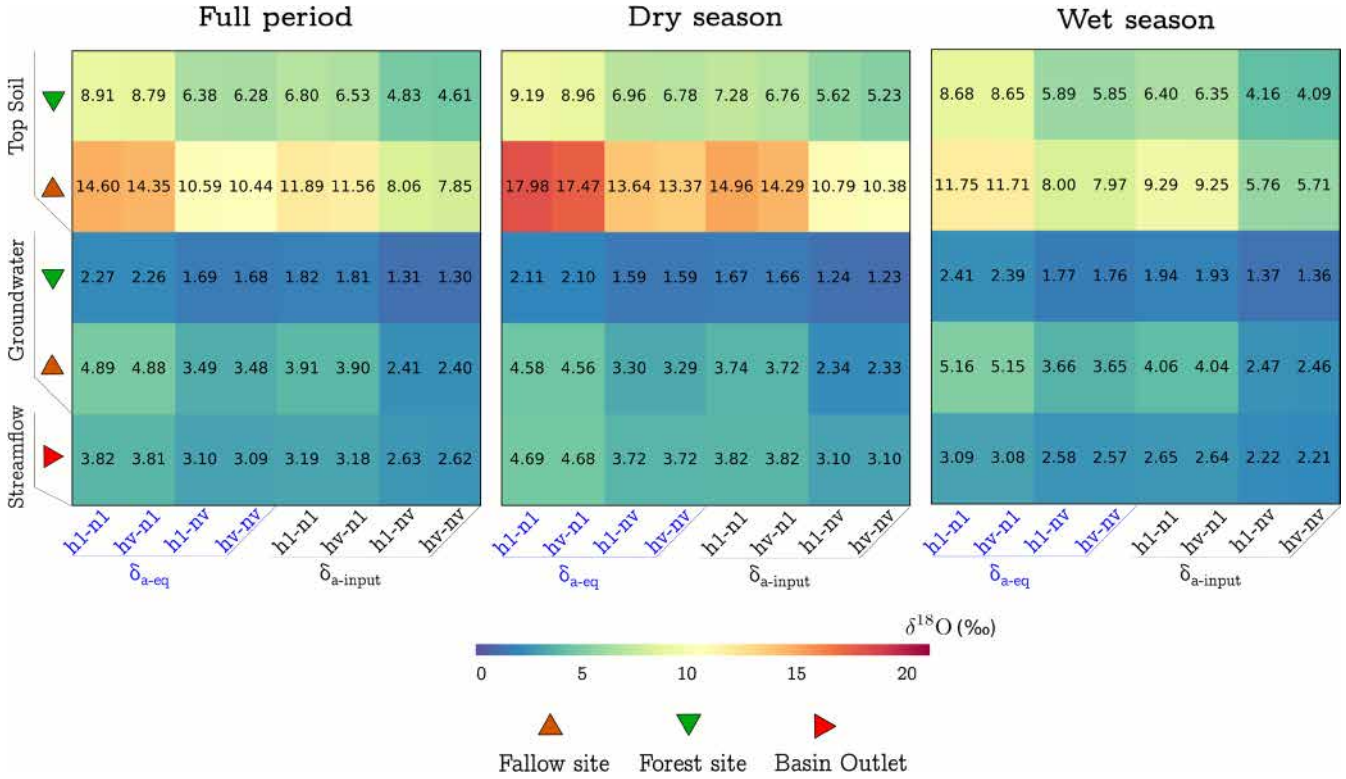

FIGURE 6 | Intra-model dispersion (ID) of $\delta^{18}O$ (‰) time series across physical parametrizations for various conceptualizations of soil evaporative fractionation in the C-G model (overall conceptual framework). The dispersion is shown for topsoil (top rows) and groundwater (centre rows) at fallow (orange marker) and forest (green marker) sites, as well as for stream discharge at the basin outlet (red marker at the bottom row), for the full simulation period (left column), and distinguishing between dry (centre column) and rainy (right column) seasons.

dispersion, with *hs* reaching 1.5‰ and 1.6‰, and *n* reaching 10‰ and 28.5‰, while δ_a shows a slight increase, with 1.0‰ and 2.9‰ respectively (Figures S4–S5).

3.2 | Conceptual Sensitivity

The pairwise impact of changing the C-G conceptual framework (see Section 2.3.2) over the entire simulation period, is summarised in Figure 7. Differences in $\delta^{18}O$ outputs between frameworks pairs are consistently larger in the topsoil under fallow than forest, a pattern also observed in groundwater, although with less marked contrasts. For streamflow, metrics remain low across all frameworks, staying below 0.5‰ and comparable to groundwater under forest. This trend persists seasonally, becoming more evident during the dry period (see Supporting Information). This figure also reveals distinct four-cell colour sectors with similar metric values, reaffirming that variations in *hs* formulations exert minimal impact on differences between simulated isotopic series. Instead, these differences are mainly driven by the C-G input variables δ_a and *n* when comparing isotopic series across conceptual frameworks.

For all $\delta^{18}O$ outputs in topsoil, groundwater and stream, highest conceptual sensitivity values occur in top-right and/or bottom-left sectors, suggesting largest changes in $\delta^{18}O$ simulations happen moving from the simplest ($h1$-$n1$-δ_{a-eq}), to the most sophisticated conceptual framework (hv-nv-$\delta_{a-input}$). When considering one conceptualization change at a time among *hs*, *n* and δ_a, at the fallow site (topsoil and groundwater) and at the outlet, the largest change in $\delta^{18}O$ arises from the choice of the *n* formulation ($n1$ vs. nv), under a fixed δ_a setting (δ_{a-eq} or $\delta_{a-input}$), followed by the choice of δ_a under a fixed *n* setting. At the forest site, the impact of the *n* formulation is twice smaller for both topsoil and groundwater $\delta^{18}O$ signature as compared to the fallow site, making the choice of δ_a setting the most

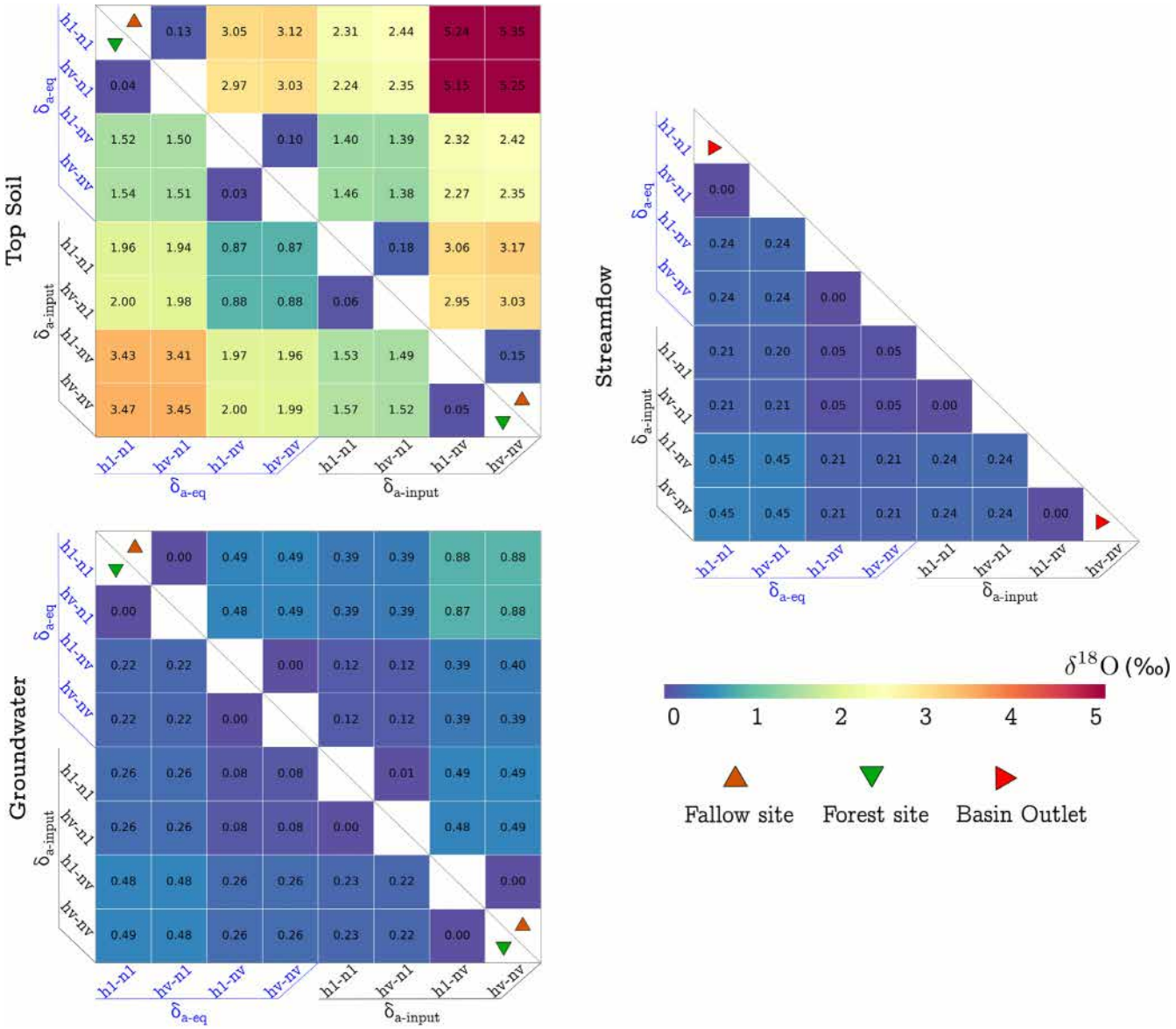

FIGURE 7 | Pairwise difference metric of $\delta^{18}O$ time series from models using different soil evaporative fractionation conceptualizations. Heatmaps are shown for topsoil (upper part of the first column) and groundwater (lower part of the first column), segmented by land cover type (fallow on top, forest below). The panel in the second column presents the corresponding values at the Bétérou basin outlet.

influential individual change under this land cover (for a given n formulation), followed by the choice of n setting (for a given δ_a formulation). Smaller differences are found when shifting from $nv\text{-}\delta_{a-eq}$ to $n1\text{-}\delta_{a-input}$ conceptualisation, and, as highlighted in previous sections, changing only the hs formulation has little to no impact (blue cells near the diagonals). A similar pattern with substantially higher values appears for d-excess (Figure S6).

4 | Discussion

From the above results, we first explore how the most influential parameters can help uncover the hydrological processes driving the simulated isotopic signatures. We then discuss land cover control on flux partitioning, as suggested by the reported sensitivities of δ^{18}O time series, both within and across conceptual frameworks of evaporative fractionation, and accounting for seasonality and the diverse compartments. We also discuss how the choice of the conceptual framework modifies the parametric sensitivities, and how the sensitivity to non-isotopic parameters compares with the sensitivity to the conceptualization of isotopic fractionation. Finally, our results are recast in the broader context of model-data fusion approaches for investigating ecohydrological processes using stable isotopes.

4.1 | Insights From Parametric Sensitivity Analysis on Hydrological Processes and Land Cover Controls

Our results show a high sensitivity of the isotopic outputs to parameters controlling water storage and transfer in the topsoil (λ_{BC-L1}, θr_{L1}, θ_{L1} and ψae_{L1}), suggesting that the isotopic composition in this compartment strongly depends on how much water is stored and how long it remains before being transferred to deeper soil layers, taken up by plants or lost to evaporation. This pattern echoes previous studies demonstrating that isotopic composition in the uppermost soil layers can vary significantly, often exceeding that of precipitation, due to evaporative enrichment modulated by residence time and storage volume buffering isotopic changes (Penna et al. 2018; Sprenger et al. 2016). In addition to these soil-based hydrological controls, our results show that vegetation cover itself contributes to the variability in soil water isotopic composition. In particular, the contrasting sensitivity patterns between forest and fallow sites suggest different dominant processes. Under fallow cover, the imprint of deeper water transit is most visible, as parameters controlling storage and flow beyond the upper decimetres of soil (D_{L2}, θ_{L2}, K_{L2}, θ_{L3} and K_{L3}) are much more influential than under forest cover, where they have little or no impact on the topsoil isotopic signal. In contrast, under forest cover, the high sensitivity of parameters related to stomatal conductance (gs_*) reflects the predominant role of root uptake in shaping water availability in the topsoil layer. Keeping in mind that no a priori rooting depth per vegetation type is prescribed in this version of the model (see Section 2.1.1), this result is suggestive of spatial and temporal differences in selective root water uptake profiles between vegetation types as a tight interplay between of foliar timing (driving demand and here prescribed for each land cover) and local water flow paths (driving supply), as has been well documented in the literature (Allen et al. 2019; Benettin et al. 2022; Sprenger and Allen 2020). Moreover, the significant sensitivities of topsoil δ^{18}O time series to the K_{Beer} parameter in both fallow and forest sites with slightly greater sensitivity under fallow cover due to reduced shading from lower LAI, is consistent with reported vegetation-driven changes in soil surface evaporation, and hence evaporative fractionation (Smith et al. 2022; Sprenger et al. 2016).

Within the groundwater compartment which may span all subsurface layers depending on hydrological conditions, δ^{18}O shows pronounced sensitivity to storage in the deepest soil layer (θ_{L3}), with depths of 10–30 m (Table 2), under both fallow and forest, indicating deep storage mainly controls groundwater isotopic composition baseline. Attenuated sensitivities of other parameters suggest strong dampening of soil water isotopic signals, consistent with groundwater compartments having high inertia that substantially reduces isotopic variability of recharge waters upon mixing with stored water (Kuppel et al. 2018a; Sprenger et al. 2016, 2019). Lack of sensitivity to hydraulic conductivity (K_{L3}) under forest suggests more limited lateral water movement in this cover type, while sensitivity under fallow indicates lateral flow contributes to isotopic variation (potentially due to higher groundwater storage due to lower transpiration, not shown). Sensitivity to physical parameters in the upper layers (L1 and L2) under fallow shows the role of vertical connectivity in shaping the groundwater isotopic signal. Conversely, marked groundwater δ^{18}O sensitivity to stomatal conductance parameters under forest indicates dominant plant water uptake influence, whereas low sensitivity under fallow suggests this compartment is relatively unaffected by vegetation uptake.

At the basin outlet, the parametric sensitivity of stream δ^{18}O reflects the larger spatial coverage of fallow vegetation in the model (approximately three times that of forest, see Figure 2b). Indeed, at this integrative scale we find again a predominant sensitivity to some parameters controlling soil water dynamics at the cell level under this cover (K_{L3}, K_{L2}, θ_{L3}, θ_{L2}), which were only dominant under fallow vegetation as seen in topsoil and groundwater (see Sections 3.1 and 4.1). Although model-based, these results agree with the broader understanding that river networks integrate contributions from smaller units. Such cross-scale propagation makes plot-scale processes essential to interpret basin-scale dynamics, from (sub)surface water budgets in representative land cover types (such as the two grid 1 km^2 grid cells considered here) to ecohydrological functioning at the basin scale (Benettin et al. 2022; Bracken et al. 2013; Sprenger and Allen 2020).

4.2 | Interaction Between Conceptual and Parametric Sensitivity

The model used in this study (EcH$_2$O-iso, Section 2.1.1) adapts the C–G formulation to calculate kinetic fractionation in soils and allows the incorporation of a detailed conceptualization of soil moisture state directly into its structure, using a mechanistic and explicit approach for variables such as the aerodynamic regime factor above the liquid–vapour interface (n) and the relative humidity in soil pores (hs), both described in Section 2.1.2.

As shown in Table S1, to our knowledge no other tracer-enabled hydrological model combines this flexibility in process description with a process-based 3D ecohydrological description of water pathways and evaporation partitioning, let alone applied in an ET-driven setting such as the tropical watershed studied here. Semi- or fully-distributed models typically prescribe fixed n values or directly deriving hs from atmospheric relative humidity, which is given as an input forcing, without accounting for the dynamic feedback between soil moisture and internal pore humidity (Correa et al. 2020; Stadnyk et al. 2013; Watson et al. 2024), while refined formulation have been used in 1D approaches, probably owing to the associated computational cost (e.g., Braud et al. 2005; Haverd and Cuntz 2010). This flexible formulation of key variables in this study, along with the option to prescribe δ_a as a model input and thus go beyond the standard assumption of isotopic equilibrium, allowed here to quantify the impacts of conceptual choices by considering two aspects: first, how the above-discussed parametric sensitivity of isotopic signatures within model compartments varies between conceptual frameworks (i.e., change of intra-framework-parametric-sensitivity, Section 3.1), and second, how changes in fractionation model formulations affect outputs on average across all parameter sets (i.e., conceptual sensitivity or inter-framework sensitivity, Section 3.2).

Regarding the first aspect, our results suggest that parametric sensitivities of modelled isotopic outputs can be reduced when simulations are performed using conceptual frameworks relying on more flexible formulation (i.e., hv, nv and $\delta_{a-input}$). When comparing the impact of modifying individual components across frameworks, changing n generally produced the largest effect, not only in reducing parametric sensitivity (Figures 5 and 6), but also in altering δ^{18}O signatures for comparable parametrizations (Figure 7), followed by δ_a and hs. For n and hs, reductions in parametric sensitivity are associated with the use of formulations based in soil moisture state, rather than fixed maximum values such as $hs=1$ ($h1$) and $n=1$ ($n1$), which directly affect the calculation of kinetic fractionation (see Equation 11). For δ_a, the reduction is attributed to the dynamic representation of a more depleted isotopic signal of atmospheric moisture during the dry season in $\delta_{a-input}$ (mean −14.75‰ vs. −11.03‰ for δ_{a-eq}), since both approaches show similar values in the wet season (mean −12.94‰ vs. −13.19‰). On the other hand, the seasonal variation in sensitivity, particularly evident in the soil physical parameters (λ_{BC-L1}, D_{L1}, θ_{L1} and θr_{L1}) of the topsoil compartment under fallow cover (Figure S2), can be explained by the contrasting moisture and evaporative conditions between the dry and wet seasons, as also reflected in the shifts in the parametric sensitivity of d-excess (see Supporting Information). This variation shows the imprint of variable n, which tends to reach its highest values during the dry period as topsoil moisture approaches residual levels ($\theta = \theta_r$ in Equation 12), thereby driving the observed increases in sensitivity. The less marked seasonal shift under forest cover reflects the influence of different dominant processes, as discussed in Section 4.1. However, even with these flexible formulations, the parametric sensitivity of isotopic signatures remains significant (≥0.5‰) for many parameters, even when using the most flexible conceptualizations (e.g., hv-nv-$\delta_{a-input}$). This arises because those parameters drive water and energy fluxes to which isotopic signatures are intrinsically linked (see Section 4.1).

As for the second aspect, the conceptual sensitivity analysis shows that the biggest differences in δ^{18}O simulations are found when comparing the most flexible and the most simplified formulation of the evaporative fractionation (hv-nv-$\delta_{a-input}$ vs. $h1$-$n1$-δ_{a-eq}), particularly evident in the topsoil compartment under fallow cover. These differences are similar in magnitude to the reductions in δ^{18}O dispersion between the two formulations and comparable to the largest individual parametric uncertainty identified in this compartment (Figures 5 and 6), illustrating that a straightforward conceptual change, at minimal calculation cost, can substantially influence isotopic simulations.

Taken together, it appears that moving from simplified to more process-based formulations reduces parameter sensitivity and dispersion in modelled isotopic outputs. This suggests that, despite known challenges in accurately determining kinetic separation factors (Horita et al. 2008; Quade et al. 2018), a more flexible representation of key C-G variables (i.e., hs, n and δ_a) improve the capacity of the model to capture changing regimes of evaporative fractionation. More broadly, a refined quantification of C-G variables may reduce the influence of poorly known (at spatialized scales) and yet classical ecohydrological parameters (e.g., porosity, hydraulic conductivity, retention curve factors, stomatal conductance) when isotopic information content is used for model constraint and evaluation.

4.3 | Implications for Data-Informed Modelling Approaches Using Stable Isotopes

It is well established that in ecohydrological modelling, there are no universally valid approaches, and that selecting an appropriate model structure, along with the values and interpretation of its parameters (whether physically based or not) depends on the scientific questions and thus model purpose, in addition to basin characteristics, data availability, and underlying assumptions (Blöschl and Sivapalan 1995; Bracken et al. 2013; Holmes et al. 2023; Hrachowitz, Savenije, Blöschl, et al. 2013; McDonnell et al. 2007; Stadnyk and Holmes 2023; Turnadge and Smerdon 2014).

In this study, we deliberately used a state-of-the-art ecohydrological model in its current formulation regarding the physics of water and energy fluxes, and we focused on testing alternative conceptualizations of isotopic fractionation while the hydrological impact is addressed through model parameterization. Our results are partly both model and site-specific, and we do not consider the impact of other uncertainties associated with climatic forcings and the chosen resolution of the simulation domain. Yet, our analysis may still help guide the use of isotope-assisted models for tracking water pathways in the critical zone.

At the basin scale, the outlet plays an integrative role by collecting all water stored—then released or rapidly running off in the upstream basin and routed from individual grid cells, effectively blending together their contributions in a single isotopic signature at a given moment (Botter et al. 2010; Holmes et al. 2023; Kirchner et al. 2010). This spatial integration smooths out the local variability in isotopic fractionation otherwise reported along the subsurface profile at individual fallow and forest sites, as evidenced by limited changes in parametric sensitivity, minor

variations in $\delta^{18}O$ dispersion, and relatively homogeneous conceptual sensitivities (see Figure 7). These findings suggest that choosing the most flexible conceptual framework for fractionation leads to only a modest improvement in how effectively available isotopic data inform the model at this scale, as mixing tends to dominate over fractionation. Therefore, when studying run-off generation at the basin scale, adopting a process-based framework for estimating soil isotopic fractionation may not show up in stream isotopes, even in evaporation-dominated environments, unless stream water is substantially affected by interflow in soils and/or evaporation in riparian zones (e.g., Sprenger et al. 2017). On the other hand, at the local, cell level where soil water evaporation is a key component of the isotopic and water balance, the impact of using more flexible conceptual choices becomes more clearly distinguishable.

From a model-data perspective, where observations inform calibration, evaluation and uncertainty reduction, the choice of conceptualization of evaporative fractionation can strongly affect the calibrated "non-isotopic" parameter values, their uncertainties, and the overall performance of modelling soil and groundwater isotopic dynamics. However, as noted above, at the basin scale, where stream isotopes were analysed, this choice has only a modest impact. While this challenges the need for detailed, physically refined representations of evaporative fractionation when stream isotopes are the sole observational constraint, such refined representations remain crucial for constraining parameters at the local scale, as isotopes help better discern whether water arrives at the right place, at the right time, and with the right flow, by offering insights into its origin, age and transport pathways (McGuire and McDonnell 2015). This reinforces the value of flexible conceptual formulations for producing more realistic simulations at the local scale, enabling more reliable upscaling model responses, allowing us to achieve the right answers for the right reasons (Kirchner 2006), and thereby improving confidence in basin-scale scenario analyses, such as evaluating the effects of vegetation cover or climate change on the water cycle.

5 | Conclusions

The ability of tracer-enabled models to represent complex ecohydrological processes largely depends on how the informational value of isotopic tracers is incorporated in model-data calibration/validation methodologies. We used a state-of-the-art tracer-enabled ecohydrological model to evaluate the sensitivity of isotopic outputs to both parameter values and conceptual assumptions in the calculation of soil evaporative fractionation. We show that the isotopic signature of water in streams, soils and groundwater is equally sensitive to both types of sensitivities, but also that the magnitude of parametric sensitivity is reduced in more refined conceptualizations of fractionation. As hydrological modelling increasingly seeks to leverage the information content found in stable isotopes measurements through model calibration and evaluation, our results suggest performing preliminary sensitivity analyses not only on parameters but also related to the choice of representations of evaporative fractionation as a first step to select a fit-for-purpose model-data approach. This is especially relevant for tropical critical zones with significant ET-driven hydrology. This matters at the local scale, and, to a lesser extent, at the basin scale where refined fractionation frameworks may be helpful for more realistic simulations including water transit time estimates fluxes across and out of catchments and scenario studies on changes in vegetation cover and evaporative demand at nested scales (hillslope to basin).

Acknowledgements

This work was supported by the French national research program EC2CO (Continental and Coastal Ecosphere) through the WAWAPiso project (West African WAter Pathways: regional monitoring and hydrological modelling with stable ISOtopes). Rainfall isotope monitoring also benefited from funding by the ANR (ANR-17-CE01-0002-01). We gratefully acknowledge the IT department of the OSU Institute Pythéas (Aix–Marseille Université, INSU-CNRS) for providing access to its high-performance computing resources, and the AMMA-Catch observatory team for their collaboration and insightful discussions.

Funding

This work was supported by Agence Nationale de la Recherche (ANR-17-CE01-0002-01) and Institut National des Sciences de L'univers (INSU): EC2CO program (Continental and Coastal Ecosphere).

Data Availability Statement

The data that support the findings of this study are available from the corresponding author upon reasonable request. The code of the model EcH$_2$O-iso used in this study is available in the open repository bitbucket.org/scicirc/ech2o-iso, master branch (from commit d598f06).

References

Abbas, S. A., R. T. Bailey, J. T. White, et al. 2024. "A Framework for Parameter Estimation, Sensitivity Analysis, and Uncertainty Analysis for Holistic Hydrologic Modeling Using SWAT+." *Hydrology and Earth System Sciences* 28, no. 1: 21–48. https://doi.org/10.5194/hess-28-21-2024.

Ala-aho, P., D. Tetzlaff, J. P. McNamara, H. Laudon, and C. Soulsby. 2017. "Using Isotopes to Constrain Water Flux and Age Estimates in Snow-Influenced Catchments Using the STARR (Spatially Distributed Tracer-Aided Rainfall–Runoff) Model." *Hydrology and Earth System Sciences* 21, no. 10: 5089–5110. https://doi.org/10.5194/hess-21-5089-2017.

Allen, S. T., J. W. Kirchner, S. Braun, R. T. W. Siegwolf, and G. R. Goldsmith. 2019. "Seasonal Origins of Soil Water Used by Trees." *Hydrology and Earth System Sciences* 23, no. 2: 1199–1210. https://doi.org/10.5194/hess-23-1199-2019.

Allison, G. B., and F. W. Leaney. 1982. "Estimation of Isotopic Exchange Parameters, Using Constant-Feed Pans." *Journal of Hydrology* 55, no. 1–4: 151–161. https://doi.org/10.1016/0022-1694(82)90126-3.

Barnes, C. J., and G. B. Allison. 1983. "The Distribution of Deuterium and 18O in Dry Soils: 1. Theory." *Journal of Hydrology* 60: 141–156.

Belachew, D. L., G. Leavesley, O. David, et al. 2016. "IAEA Isotope-Enabled Coupled Catchment–Lake Water Balance Model, IWBMIso: Description and Validation." *Isotopes in Environmental and Health Studies* 52, no. 4–5: 427–442. https://doi.org/10.1080/10256016.2015.1113959.

Benettin, P., and E. Bertuzzo. 2018. "*Tran*-SAS v1.0: A Numerical Model to Compute Catchment-Scale Hydrologic Transport Using StorAge Selection Functions." *Geoscientific Model Development* 11, no. 4: 1627–1639. https://doi.org/10.5194/gmd-11-1627-2018.

Benettin, P., N. B. Rodriguez, M. Sprenger, et al. 2022. "Transit Time Estimation in Catchments: Recent Developments and Future Directions." *Water Resources Research* 58, no. 11. https://doi.org/10.1029/2022WR033096.

Birkel, C., and C. Soulsby. 2015. "Advancing Tracer-Aided Rainfall-Runoff Modelling: A Review of Progress, Problems and Unrealised Potential: Advancing Tracer-Aided Rainfall-Runoff Modelling." *Hydrological Processes* 29, no. 25: 5227–5240. https://doi.org/10.1002/hyp.10594.

Bittner, D., M. Engel, B. Wohlmuth, D. Labat, and G. Chiogna. 2021. "Temporal Scale-Dependent Sensitivity Analysis for Hydrological Model Parameters Using the Discrete Wavelet Transform and Active Subspaces." *Water Resources Research* 57, no. 10: e2020WR028511. https://doi.org/10.1029/2020WR028511.

Blöschl, G., and M. Sivapalan. 1995. "Scale Issues in Hydrological Modelling: A Review." *Hydrological Processes* 9, no. 3–4: 251–290. https://doi.org/10.1002/hyp.3360090305.

Bong, H., A. Cauquoin, A. Okazaki, et al. 2024. "Process-Based Intercomparison of Water Isotope-Enabled Models and Reanalysis Nudging Effects." *Journal of Geophysical Research: Atmospheres* 129, no. 1: e2023JD038719. https://doi.org/10.1029/2023JD038719.

Bormann, H., and B. Diekkrüger. 2003. "Possibilities and Limitations of Regional Hydrological Models Applied Within an Environmental Change Study in Benin (West Africa)." *Physics and Chemistry of the Earth, Parts A/B/C* 28, no. 33–36: 1323–1332. https://doi.org/10.1016/j.pce.2003.09.008.

Botter, G., E. Bertuzzo, and A. Rinaldo. 2010. "Transport in the Hydrologic Response: Travel Time Distributions, Soil Moisture Dynamics, and the Old Water Paradox." *Water Resources Research* 46, no. 3. https://doi.org/10.1029/2009wr008371.

Bracken, L. J., J. Wainwright, G. A. Ali, et al. 2013. "Concepts of Hydrological Connectivity: Research Approaches, Pathways and Future Agendas." *Earth-Science Reviews* 119: 17–34. https://doi.org/10.1016/j.earscirev.2013.02.001.

Braud, I., T. Bariac, P. Biron, and M. Vauclin. 2009. "Isotopic Composition of Bare Soil Evaporated Water Vapor. Part II: Modeling of RUBIC IV Experimental Results." *Journal of Hydrology* 369, no. 1–2: 17–29. https://doi.org/10.1016/j.jhydrol.2009.01.038.

Braud, I., T. Bariac, J. P. Gaudet, and M. Vauclin. 2005. "SiSPAT-Isotope, a Coupled Heat, Water and Stable Isotope (HDO and H218O) Transport Model for Bare Soil. Part I. Model Description and First Verifications." *Journal of Hydrology* 309, no. 1–4: 277–300. https://doi.org/10.1016/j.jhydrol.2004.12.013.

Cornelissen, T., B. Diekkrüger, and S. Giertz. 2013. "A Comparison of Hydrological Models for Assessing the Impact of Land Use and Climate Change on Discharge in a Tropical Catchment." *Journal of Hydrology* 498: 221–236. https://doi.org/10.1016/j.jhydrol.2013.06.016.

Correa, A., C. Birkel, J. Gutierrez, et al. 2020. "Modelling Non-Stationary Water Ages in a Tropical Rainforest: A Preliminary Spatially Distributed Assessment." *Hydrological Processes* 34, no. 25: 4776–4793. https://doi.org/10.1002/hyp.13925.

Cox, P. M., C. Huntingford, and R. J. Harding. 1998. "A Canopy Conductance and Photosynthesis Model for Use in a GCM Land Surface Scheme." *Journal of Hydrology* 212: 79–94. https://doi.org/10.1016/s0022-1694(98)00203-0.

Craig, H., and L. I. Gordon. 1965. "Deuterium and Oxygen 18 Variations in the Ocean and the Marine Atmosphere." In *Stable Isotopes in Oceanographic Studies and Paleotemperatures*. Consiglio Nazionale Delle Richerche, Laboratorio Di Geologia Nucleare.

Delattre, H., C. Vallet-Coulomb, and C. Sonzogni. 2015. "Deuterium Excess in the Atmospheric Water Vapour of a Mediterranean Coastal Wetland: Regional vs. Local Signatures." *Atmospheric Chemistry and Physics* 15, no. 17: 10167–10181. https://doi.org/10.5194/acp-15-10167-2015.

Douinot, A., D. Tetzlaff, M. Maneta, S. Kuppel, H. Schulte-Bisping, and C. Soulsby. 2019. "Ecohydrological Modelling With EcH $_2$ O-Iso to Quantify Forest and Grassland Effects on Water Partitioning and Flux Ages." *Hydrological Processes* 33, no. 16: 2174–2191. https://doi.org/10.1002/hyp.13480.

Dubbert, M., M. Cuntz, A. Piayda, C. Maguás, and C. Werner. 2013. "Partitioning Evapotranspiration – Testing the Craig and Gordon Model With Field Measurements of Oxygen Isotope Ratios of Evaporative Fluxes." *Journal of Hydrology* 496: 142–153. https://doi.org/10.1016/j.jhydrol.2013.05.033.

El-Fahem, T. 2008. "Hydrogeological Conceptualisation of a Tropical River Catchment in a Crystalline Basement Area and Transfer Into a Numerical Groundwater Flow Model—Case Study for the Upper Ouémé Catchment in Benin."

Evaristo, J., M. Kim, J. Van Haren, et al. 2019. "Characterizing the Fluxes and Age Distribution of Soil Water, Plant Water, and Deep Percolation in a Model Tropical Ecosystem." *Water Resources Research* 55, no. 4: 3307–3327. https://doi.org/10.1029/2018WR023265.

Fan, Y., G. Miguez-Macho, E. G. Jobbágy, R. B. Jackson, and C. Otero-Casal. 2017. "Hydrologic Regulation of Plant Rooting Depth." *Proceedings of the National Academy of Sciences of the United States of America* 114: 10572–10577.

Galle, S., M. Grippa, C. Peugeot, et al. 2018. "AMMA-CATCH, a Critical Zone Observatory in West Africa Monitoring a Region in Transition." *Vadose Zone Journal* 17, no. 1: 1–24. https://doi.org/10.2136/vzj2018.03.0062.

Gat, J. R. 1995. "5 Stable Isotopes of Fresh and Saline Lakes."

Gat, J. R., and Y. Levy. 1978. "Isotope Hydrology of Inland Sabkhas in the Bardawil Area, Sinai." *Limnology and Oceanography* 23, no. 5: 841–850. https://doi.org/10.4319/lo.1978.23.5.0841.

Gibson, J. J., S. J. Birks, and Y. Yi. 2016. "Stable Isotope Mass Balance of Lakes: A Contemporary Perspective." *Quaternary Science Reviews* 131: 316–328. https://doi.org/10.1016/j.quascirev.2015.04.013.

Gibson, J. J., and R. Reid. 2014. "Water Balance Along a Chain of Tundra Lakes: A 20-Year Isotopic Perspective." *Journal of Hydrology* 519: 2148–2164. https://doi.org/10.1016/j.jhydrol.2014.10.011.

Gillefalk, M., D. Tetzlaff, R. Hinkelmann, et al. 2021. "Quantifying the Effects of Urban Green Space on Water Partitioning and Ages Using an Isotope-Based Ecohydrological Model." *Hydrology and Earth System Sciences* 25, no. 6: 3635–3652. https://doi.org/10.5194/hess-25-3635-2021.

Good, S. P., K. Soderberg, K. Guan, E. G. King, T. M. Scanlon, and K. K. Caylor. 2014. "δ^2 H Isotopic Flux Partitioning of Evapotranspiration Over a Grass Field Following a Water Pulse and Subsequent Dry Down." *Water Resources Research* 50, no. 2: 1410–1432. https://doi.org/10.1002/2013WR014333.

Harman, C. J., and E. Xu Fei. 2024. "Mesas.Py v1.0: A Flexible Python Package for Modeling Solute Transport and Transit Times Using StorAge Selection Functions." *Geoscientific Model Development* 17, no. 2: 477–495. https://doi.org/10.5194/gmd-17-477-2024.

Haverd, V., and M. Cuntz. 2010. "Soil-Litter-Iso: Aone-Dimensional Model for Coupled Transport of Heat, Water and Stable Isotopesin Soil With a Litter Layer and Root Extraction." *Journal of Hydrology* 388, no. 3–4: 438–455. https://doi.org/10.1016/j.jhydrol.2010.05.029.

He, Z., K. Unger-Shayesteh, S. Vorogushyn, et al. 2019. "Constraining Hydrological Model Parameters Using Water Isotopic Compositions in a Glacierized Basin, Central Asia." *Journal of Hydrology* 571: 332–348. https://doi.org/10.1016/j.jhydrol.2019.01.048.

Holmes, T. L., T. A. Stadnyk, M. Asadzadeh, and J. J. Gibson. 2023. "Guidance on Large Scale Hydrologic Model Calibration With Isotope Tracers." *Journal of Hydrology* 621: 129604. https://doi.org/10.1016/j.jhydrol.2023.129604.

Horita, J., K. Rozanski, and S. Cohen. 2008. "Isotope Effects in the Evaporation of Water: A Status Report of the Craig–Gordon Model."

Isotopes in Environmental and Health Studies 44, no. 1: 23–49. https://doi.org/10.1080/10256010801887174.

Horita, J., and D. J. Wesolowski. 1994. "Liquid-Vapor Fractionation of Oxygen and Hydrogen Isotopes of Water From the Freezing to the Critical Temperature." *Geochimica et Cosmochimica Acta* 58, no. 16: 3425–3437. https://doi.org/10.1016/0016-7037(94)90096-5.

Hrachowitz, M., H. Savenije, T. A. Bogaard, D. Tetzlaff, and C. Soulsby. 2013. "What Can Flux Tracking Teach Us About Water Age Distribution Patterns and Their Temporal Dynamics?" *Hydrology and Earth System Sciences* 17, no. 2: 533–564. https://doi.org/10.5194/hess-17-533-2013.

Hrachowitz, M., H. H. G. Savenije, G. Blöschl, et al. 2013. "A Decade of Predictions in Ungauged Basins (PUB)—A Review." *Hydrological Sciences Journal* 58, no. 6: 1198–1255. https://doi.org/10.1080/02626667.2013.803183.

IAEA. 2023. *Towards Best Practices in Isotope-Enabled Hydrological Modelling Applications (First Edition)*. International Atomic Energy Agency.

Jarvis, P. G. 1976. "The Interpretation of the Variations in Leaf Water Potential and Stomatal Conductance Found in Canopies in the Field." *Philosophical Transactions of the Royal Society of London. B, Biological Sciences* 273, no. 927: 593–610. https://doi.org/10.1098/rstb.1976.0035.

Jasechko, S. 2019. "Global Isotope Hydrogeology—Review." *Reviews of Geophysics* 57, no. 3: 835–965. https://doi.org/10.1029/2018RG000627.

Kirchner, J. W. 2006. "Getting the Right Answers for the Right Reasons: Linking Measurements, Analyses, and Models to Advance the Science of Hydrology." *Water Resources Research* 42, no. 3: 2005WR004362. https://doi.org/10.1029/2005WR004362.

Kirchner, J. W., and S. T. Allen. 2020. "Seasonal Partitioning of Precipitation Between Streamflow and Evapotranspiration, Inferred From End-Member Splitting Analysis." *Hydrology and Earth System Sciences* 24, no. 1: 17–39. https://doi.org/10.5194/hess-24-17-2020.

Kirchner, J. W., D. Tetzlaff, and C. Soulsby. 2010. "Comparing Chloride and Water Isotopes as Hydrological Tracers in Two Scottish Catchments." *Hydrological Processes* 24, no. 12: 1631–1645. https://doi.org/10.1002/hyp.7676.

Knighton, J., S. M. Saia, C. K. Morris, J. A. Archiblad, and M. T. Walter. 2017. "Ecohydrologic Considerations for Modeling of Stable Water Isotopes in a Small Intermittent Watershed." *Hydrological Processes* 31, no. 13: 2438–2452. https://doi.org/10.1002/hyp.11194.

Knighton, J., V. Souter-Kline, T. Volkmann, et al. 2019. "Seasonal and Topographic Variations in Ecohydrological Separation Within a Small, Temperate, Snow-Influenced Catchment." *Water Resources Research* 55, no. 8: 6417–6435. https://doi.org/10.1029/2019WR025174.

Kotchoni, D. O. V., J.-M. Vouillamoz, F. M. A. Lawson, P. Adjomayi, M. Boukari, and R. G. Tay-lor. 2019. "Relationships Between Rainfall and Groundwater Recharge in Seasonal-ly Humid Benin: A Comparative Analysis of Long-Term Hydrographs in Sedimentary and Crystalline Aquifers." *Hydrogeology Journal* 27, no. 2: 447–457. https://doi.org/10.1007/s10040-018-1806-2.

Kumar, B., and R. P. Nachiappan. 1999. "On the Sensitivity of Craig and Gordon Model for the Estimation of the Isotopic Composition of Lake Evaporates." *Water Resources Research* 35, no. 5: 1689–1691. https://doi.org/10.1029/1999WR900011.

Kuppel, S., D. Tetzlaff, M. P. Maneta, and C. Soulsby. 2018a. "EcH2o-Iso 1.0: Water Isotopes and Age Tracking in a Process-Based, Distributed Ecohydrological Model." *Geoscientific Model Development* 11, no. 7: 3045–3069. https://doi.org/10.5194/gmd-11-3045-2018.

Kuppel, S., D. Tetzlaff, M. P. Maneta, and C. Soulsby. 2018b. "What Can We Learn From Multi-Data Calibration of a Process-Based Ecohydrological Model?" *Environmental Modelling & Software* 101: 301–316. https://doi.org/10.1016/j.envsoft.2018.01.001.

Le Lay, M., S. Galle, G. M. Saulnier, and I. Braud. 2007. "Exploring the Relationship Between Hydroclimatic Stationarity and Rainfall-Runoff Model Parameter Stability: A Case Study in West Africa." *Water Resources Research* 43, no. 7. https://doi.org/10.1029/2006WR005257.

Lee, T., and R. Pielke. 1991. "Estimating the Soil Surface Specific Humidity." *Journal of Applied Meteorology* 31: 480–484.

Li, D., Q. Ju, P. Jiang, et al. 2023. "Sensitivity Analysis of Hydrological Model Parameters Based on Improved Morris Method With the Double-Latin Hypercube Sampling." *Hydrology Research* 54, no. 2: 220–232. https://doi.org/10.2166/nh.2023.109.

Lin, Y., and J. Horita. 2016. "An Experimental Study on Isotope Fractionation in a Mesoporous Silica-Water System With Implications for Vadose-Zone Hydrology." *Geochimica et Cosmochimica Acta* 184: 257–271. https://doi.org/10.1016/j.gca.2016.04.029.

Lohou, F., L. Kergoat, F. Guichard, et al. 2014. "Surface Response to Rain Events Throughout the West African Monsoon." *Atmospheric Chemistry and Physics* 14, no. 8: 3883–3898. https://doi.org/10.5194/acp-14-3883-2014.

Maneta, M. P., and N. L. Silverman. 2013. "A Spatially Distributed Model to Simulate Water, Energy, and Vegetation Dynamics Using Information From Regional Climate Models." *Earth Interactions* 17, no. 11: 1–44. https://doi.org/10.1175/2012EI000472.1.

Mathieu, R., and T. Bariac. 1996. "A Numerical Model for the Simulation of Stable Isotope Profiles in Drying Soils." *Journal of Geophysical Research: Atmospheres* 101, no. D7: 12685–12696. https://doi.org/10.1029/96JD00223.

McDonnell, J. J., M. Sivapalan, K. Vaché, et al. 2007. "Moving Beyond Heterogeneity and Process Complexity: A New Vision for Watershed Hydrology." *Water Resources Research* 43, no. 7: 2006WR005467. https://doi.org/10.1029/2006WR005467.

McGuire, K. J., and J. J. McDonnell. 2006. "A Review and Evaluation of Catchment Transit Time Modeling." *Journal of Hydrology* 330, no. 3–4: 543–563. https://doi.org/10.1016/j.jhydrol.2006.04.020.

McGuire, K. J., and J. J. McDonnell. 2015. "Tracer Advances in Catchment Hydrology." *Hydrological Processes* 29, no. 25: 5135–5138. https://doi.org/10.1002/hyp.10740.

McKay, M. D., R. J. Beckman, and W. J. Conover. 1979. "A Comparison of Three Methods for Selecting Values of Input Variables in the Analysis of Output From a Computer Code." *Technometrics* 21, no. 2: 239. https://doi.org/10.2307/1268522.

Meira Neto, A. A., M. Kim, and P. A. Troch. 2022. "Physical Interpretation of Time-Varying StorAge Selection Functions in a Bench-Scale Hillslope Experiment via Geophysical Imaging of Ages of Water." *Water Resources Research* 58, no. 4: e2021WR030950. https://doi.org/10.1029/2021WR030950.

Mercer, J. J., D. T. Liefert, and D. G. Williams. 2020. "Atmospheric Vapour and Precipitation Are Not in Isotopic Equilibrium in a Continental Mountain Environment." *Hydrological Processes* 34, no. 14: 3078–3101. https://doi.org/10.1002/hyp.13775.

Merlivat, L. 1978. "Molecular Diffusivities of H2 16O, HD16O, and H2 18O in Gases." *Journal of Chemical Physics* 69, no. 6: 2864–2871. https://doi.org/10.1063/1.436884.

Miguez-Macho, G., and Y. Fan. 2021. "Spatiotemporal Origin of Soil Water Taken Up by Vegetation." *Nature* 598, no. 7882: 624–628. https://doi.org/10.1038/s41586-021-03958-6.

Morris, M. D. 1991. "Factorial Sampling Plans for Preliminary Computational Experiments." *Technometrics* 33, no. 2: 161–174. https://doi.org/10.1080/00401706.1991.10484804.

Muñoz Sabater, J. 2019. "ERA5-Land Monthly Averaged Data From 1950 to Present [Dataset]." Copernicus Climate Change Service (C3S) Climate Data Store (CDS). https://doi.org/10.24381/cds.e2161bac.

NASA JPL. 2013. "NASA Shuttle Radar Topography Mission Global 30 Arc Second [Dataset]." NASA EOSDIS Land Processes Distributed Active Archive Center. https://doi.org/10.5067/MEaSUREs/SRTM/SRTMGL30.002.

Neill, A. J., C. Birkel, M. P. Maneta, D. Tetzlaff, and C. Soulsby. 2021. "Structural Changes to Forests During Regeneration Affect Water Flux Partitioning, Water Ages and Hydrological Connectivity: Insights From Tracer-Aided Ecohydrological Modelling." *Hydrology and Earth System Sciences* 25, no. 9: 4861–4886. https://doi.org/10.5194/hess-25-4861-2021.

Penchenat, T., F. Vimeux, V. Daux, et al. 2020. "Isotopic Equilibrium Between Precipitation and Water Vapor in Northern Patagonia and Its Consequences on δ^{18} $O_{cellulose}$ Estimate." *Journal of Geophysical Research: Biogeosciences* 125, no. 3: e2019JG005418. https://doi.org/10.1029/2019JG005418.

Penna, D., L. Hopp, F. Scandellari, et al. 2018. "Ideas and Perspectives: Tracing Terrestrial Ecosystem Water Fluxes Using Hydrogen and Oxygen Stable Isotopes – Challenges and Opportunities From an Interdisciplinary Perspective." *Biogeosciences* 15, no. 21: 6399–6415. https://doi.org/10.5194/bg-15-6399-2018.

Pfahl, S., and H. Wernli. 2009. "Lagrangian Simulations of Stable Isotopes in Water Vapor: An Evaluation of Nonequilibrium Fractionation in the Craig-Gordon Model." *Journal of Geophysical Research: Atmospheres* 114, no. D20: 2009JD012054. https://doi.org/10.1029/2009JD012054.

Quade, M., N. Brüggemann, A. Graf, J. Vanderborght, H. Vereecken, and Y. Rothfuss. 2018. "Investigation of Kinetic Isotopic Fractionation of Water During Bare Soil Evaporation." *Water Resources Research* 54, no. 9: 6909–6928. https://doi.org/10.1029/2018WR023159.

Rinaldo, A., P. Benettin, C. J. Harman, et al. 2015. "Storage Selection Functions: A Coherent Framework for Quantifying How Catchments Store and Release Water and Solutes." *Water Resources Research* 51, no. 6: 4840–4847. https://doi.org/10.1002/2015WR017273.

Saltelli, A., M. Ratto, T. Andres, et al. 2007. *Global Sensitivity Analysis. The Primer*. 1st ed. Wiley. https://doi.org/10.1002/9780470725184.

Séguis, L., B. Kamagaté, G. Favreau, et al. 2011. "Origins of Streamflow in a Crystalline Basement Catchment in a Sub-Humid Sudanian Zone: The Donga Basin (Benin, West Africa)." *Journal of Hydrology* 402, no. 1–2: 1–13. https://doi.org/10.1016/j.jhydrol.2011.01.054.

Smith, A., D. Tetzlaff, L. Kleine, M. Maneta, and C. Soulsby. 2021. "Quantifying the Effects of Land Use and Model Scale on Water Partitioning and Water Ages Using Tracer-Aided Ecohydrological Models." *Hydrology and Earth System Sciences* 25, no. 4: 2239–2259. https://doi.org/10.5194/hess-25-2239-2021.

Smith, A., D. Tetzlaff, L. Kleine, M. P. Maneta, and C. Soulsby. 2020. "Isotope-Aided Modelling of Ecohydrologic Fluxes and Water Ages Under Mixed Land Use in Central Europe: The 2018 Drought and Its Recovery." *Hydrological Processes* 34, no. 16: 3406–3425. https://doi.org/10.1002/hyp.13838.

Smith, A., D. Tetzlaff, J. Landgraf, M. Dubbert, and C. Soulsby. 2022. "Modelling Temporal Variability of in Situ Soil Water and Vegetation Isotopes Reveals Ecohydrological Couplings in a Riparian Willow Plot." *Biogeosciences* 19, no. 9: 2465–2485. https://doi.org/10.5194/bg-19-2465-2022.

Smith, A., D. Tetzlaff, H. Laudon, M. Maneta, and C. Soulsby. 2019. "Assessing the Influence of Soil Freeze–Thaw Cycles on Catchment Water Storage–Flux–Age Interactions Using a Tracer-Aided Ecohydrological Model." *Hydrology and Earth System Sciences* 23, no. 8: 3319–3334. https://doi.org/10.5194/hess-23-3319-2019.

Smith, A., D. Tetzlaff, and C. Soulsby. 2018. "Using StorAge Selection Functions to Quantify Ecohydrological Controls on the Time-Variant Age of Evapotranspiration, Soil Water, and Recharge." *Hydrology and Earth System Sciences Discussions*: 1–25. https://doi.org/10.5194/hess-2018-57.

Smith, A., C. Welch, and T. Stadnyk. 2016. "Assessment of a Lumped Coupled Flow-Isotope Model in Data Scarce Boreal Catchments." *Hydrological Processes* 30, no. 21: 3871–3884. https://doi.org/10.1002/hyp.10835.

Snarski, J. W., S. Kuppel, C. Caridad, and J. Knighton. 2025. "Growing Season Precipitation Percolates to Groundwater Past Older Water in Storage Across a Temperate Agricultural Catchment." *Water Resources Research* 61, no. 10: e2024WR038869. https://doi.org/10.1029/2024WR038869.

Soderberg, K., S. P. Good, L. Wang, and K. Caylor. 2012. "Stable Isotopes of Water Vapor in the Vadose Zone: A Review of Measurement and Modeling Techniques." *Vadose Zone Journal* 11, no. 3. https://doi.org/10.2136/vzj2011.0165.

Sohier, H., J.-L. Farges, and H. Piet-Lahanier. 2014. "Improvement of the Representativity of the Morris Method for Air-Launch-To-Orbit Separation." *IFAC Proceedings Volumes* 47, no. 3: 7954–7959. https://doi.org/10.3182/20140824-6-ZA-1003.01968.

Sprenger, M., and S. T. Allen. 2020. "What Ecohydrologic Separation Is and Where we Can Go With It." *Water Resources Research* 56, no. 7: e2020WR027238. https://doi.org/10.1029/2020WR027238.

Sprenger, M., H. Leistert, K. Gimbel, and M. Weiler. 2016. "Illuminating Hydrological Processes at the Soil-Vegetation-Atmosphere Interface With Water Stable Isotopes." *Reviews of Geophysics* 54: 674–704.

Sprenger, M., C. Stumpp, M. Weiler, et al. 2019. "The Demographics of Water: A Review of Water Ages in the Critical Zone." *Reviews of Geophysics* 57, no. 3: 800–834. https://doi.org/10.1029/2018RG000633.

Sprenger, M., D. Tetzlaff, J. Buttle, H. Laudon, and C. Soulsby. 2018. "Water Ages in the Critical Zone of Long-Term Experimental Sites in Northern Latitudes." *Hydrology and Earth System Sciences* 22, no. 7: 3965–3981. https://doi.org/10.5194/hess-22-3965-2018.

Sprenger, M., D. Tetzlaff, C. Tunaley, J. Dick, and C. Soulsby. 2017. "Evaporation Fractionation in a Peatland Drainage Network Affects Stream Water Isotope Composition." *Water Resources Research* 53, no. 1: 851–866. https://doi.org/10.1002/2016WR019258.

Stadnyk, T. A., C. Delavau, N. Kouwen, and T. W. D. Edwards. 2013. "Towards Hydrological Model Calibration and Validation: Simulation of Stable Water Isotopes Using the isoWATFLOOD Model." *Hydrological Processes* 27, no. 25: 3791–3810. https://doi.org/10.1002/hyp.9695.

Stadnyk, T. A., and T. L. Holmes. 2023. "Large Scale Hydrologic and Tracer Aided Modelling: A Review." *Journal of Hydrology* 618: 129177. https://doi.org/10.1016/j.jhydrol.2023.129177.

Stewart, M. K. 1975. "Stable Isotope Fractionation due to Evaporation and Isotopic Exchange of Falling Waterdrops: Applications to Atmospheric Processes and Evaporation of Lakes." *Journal of Geophysical Research* 80, no. 9: 1133–1146. https://doi.org/10.1029/JC080i009p01133.

Tappan, G. G., W. M. Cushing, S. E. Cotillon, et al. 2016. "West Africa Land Use Land Cover Time Series: U.S. Geological Survey Data Release [Dataset]." U.S. Geological Survey. https://doi.org/10.5066/F73N21JF.

Tetzlaff, D., J. Buttle, S. K. Carey, K. McGuire, H. Laudon, and C. Soulsby. 2015. "Tracer-Based Assessment of Flow Paths, Storage and Runoff Generation in Northern Catchments: A Review." *Hydrological Processes* 29, no. 16: 3475–3490. https://doi.org/10.1002/hyp.10412.

Tremoy, G., F. Vimeux, S. Mayaki, et al. 2012. "A 1-Year Long δ^{18} O Record of Water Vapor in Niamey (Niger) Reveals Insightful Atmospheric Processes at Different Timescales." *Geophysical Research Letters* 39, no. 8: 2012GL051298. https://doi.org/10.1029/2012GL051298.

Turnadge, C., and B. D. Smerdon. 2014. "A Review of Methods for Modelling Environmental Tracers in Groundwater: Advantages of Tracer Concentration Simulation." *Journal of Hydrology* 519: 3674–3689. https://doi.org/10.1016/j.jhydrol.2014.10.056.

Vouillamoz, J. M., F. M. A. Lawson, N. Yalo, and M. Descloitres. 2015. "Groundwater in Hard Rocks of Benin: Regional Storage and Buffer

Capacity in the Face of Change." *Journal of Hydrology* 520: 379–386. https://doi.org/10.1016/j.jhydrol.2014.11.024.

Watson, A., S. Kralisch, J. Miller, et al. 2024. "Advancing Isotope-Enabled Hydrological Modelling for Ungauged Calibration of Data-Scarce Humid Tropical Catchments." *Hydrological Processes* 38, no. 2: e15065. https://doi.org/10.1002/hyp.15065.

Welhan, J. A., and P. Fritz. 1977. "Evaporation Pan Isotopic Behavior as an Index of Isotopic Evaporation Conditions." *Geochimica et Cosmochimica Acta* 41, no. 5: 682–686. https://doi.org/10.1016/0016-7037(77)90306-4.

Xiao, W., X. Lee, Y. Hu, et al. 2017. "An Experimental Investigation of Kinetic Fractionation of Open-Water Evaporation Over a Large Lake." *Journal of Geophysical Research: Atmospheres* 122, no. 21: 11651–11663. https://doi.org/10.1002/2017JD026774.

Xiao, W., Z. Wei, and X. Wen. 2018. "Evapotranspiration Partitioning at the Ecosystem Scale Using the Stable Isotope Method—A Review." *Agricultural and Forest Meteorology* 263: 346–361. https://doi.org/10.1016/j.agrformet.2018.09.005.

Yang, X., D. Tetzlaff, C. Müller, K. Knöller, D. Borchardt, and C. Soulsby. 2023. "Upscaling Tracer-Aided Ecohydrological Modeling to Larger Catchments: Implications for Process Representation and Heterogeneity in Landscape Organization." *Water Resources Research* 59, no. 3: e2022WR033033. https://doi.org/10.1029/2022WR033033.

Yoshimura, K., M. Kanamitsu, D. Noone, and T. Oki. 2008. "Historical Isotope Simulation Using Reanalysis Atmospheric Data." *Journal of Geophysical Research* 113, no. D19: D19108. https://doi.org/10.1029/2008JD010074.

Supporting Information

Additional supporting information can be found online in the Supporting Information section. **Data S1:** hyp70337-sup-0001-Supinfo.docx.